Effect of surface temperature on quantum dynamics of H2 on Cu(111) using a chemically accurate potential energy surface

Joy, D.; Souvik, M.; Satrajit, A.; Spiering, P.; Meyer, J.; Somers, M.F.

The Journal of Chemical Physics

Effect of surface temperature on quantum dynamics of H_2 on Cu(111) using a chemically accurate potential energy surface

Cite as: J. Chem. Phys. **154**, 104103 (2021); https://doi.org/10.1063/5.0035830
Submitted: 31 October 2020 . Accepted: 17 February 2021 . Published Online: 08 March 2021

Joy Dutta, Souvik Mandal, Satrajit Adhikari, et al.

The Journal of Chemical Physics ARTICLE scitation.org/journal/jcp

Effect of surface temperature on quantum dynamics of H_2 on Cu(111) using a chemically accurate potential energy surface

Cite as: J. Chem. Phys. 154, 104103 (2021); doi: 10.1063/5.0035830
Submitted: 31 October 2020 • Accepted: 17 February 2021 •
Published Online: 8 March 2021

Joy Dutta,[1] Souvik Mandal,[1] Satrajit Adhikari,[1,a)] Paul Spiering,[2] Jörg Meyer,[2] and Mark F. Somers[2]

AFFILIATIONS

[1]School of Chemical Sciences, Indian Association for the Cultivation of Science, Jadavpur, Kolkata 700 032, India
[2]Leiden Institute of Chemistry, Gorlaeus Laboratories, Leiden University, P.O. Box 9502, 2300 RA Leiden, The Netherlands

[a)]**Author to whom correspondence should be addressed:** pcsa@iacs.res.in

ABSTRACT

The effect of surface atom vibrations on H_2 scattering from a Cu(111) surface at different temperatures is being investigated for hydrogen molecules in their rovibrational ground state ($v = 0, j = 0$). We assume weakly correlated interactions between molecular degrees of freedom and surface modes through a Hartree product type wavefunction. While constructing the six-dimensional effective Hamiltonian, we employ (a) a chemically accurate potential energy surface according to the static corrugation model [M. Wijzenbroek and M. F. Somers, J. Chem. Phys. **137**, 054703 (2012)]; (b) normal mode frequencies and displacement vectors calculated with different surface atom interaction potentials within a cluster approximation; and (c) initial state distributions for the vibrational modes according to Bose–Einstein probability factors. We carry out 6D quantum dynamics with the so-constructed effective Hamiltonian and analyze sticking and state-to-state scattering probabilities. The surface atom vibrations affect the chemisorption dynamics. The results show physically meaningful trends for both reaction and scattering probabilities compared to experimental and other theoretical results.

I. INTRODUCTION

Surface phenomena play important roles in various chemical and physical processes such as heterogeneous catalysis, growth of semiconductor devices, corrosion, and hydrogen storage in metals. As a result of widespread relevance, the nature and mechanism of gas phase chemical reactions on surfaces have been extensively studied experimentally[1–8] as well as theoretically[9–29] during past few decades. The theoretical developments on the computation of potential energy surfaces (PESs)[15,30,31] and the formulation of molecular dynamics methodologies have progressed substantially with the advancement of experimental techniques, particularly associative desorption and molecular beam experiments. *Ab initio* molecular dynamics (AIMD) calculations employing the specific reaction parameter (SRP) approach to density functional theory (DFT) for the dissociative chemisorption of D_2 on Cu(111) at high surface temperature (T_s = 925 K) have been performed by Nattino *et al.*,[32] whereas Rettner *et al.*[4,5,33,34] and Michealson *et al.*[3,35,36] measured experimental sticking probabilities for various initial states of H_2/D_2 (v', j')–Cu(111) systems. Recently, Wodtke and coworkers[37] experimentally observed an unusual slow channel along with the mostly common fast one for the dissociative adsorption of H_2/D_2 on Cu(111)/Cu(211) around low kinetic energies (KEs) (below 0.2 eV) of the incoming diatom at higher surface temperatures (T_s = 923 ± 3 K). Such an unusual channel indicates an interesting additional reaction mechanism, where the trapped reactant tunnels through a substantial barrier much before attaining the vibrational equilibrium state (thermal equilibrium) due to the involvement of thermal fluctuation of the Cu(111)/Cu(211) surface.

Construction of accurate PESs has been a topic of interest in the regime of molecule–surface scattering processes. Wiesenekker, Kroes, and Baerends[38] developed a six-dimensional (6D) PES using the generalized gradient approximation (GGA) of density functional theory (DFT) for describing dissociative chemisorption of H_2 over the Cu(100) surface. On the other hand, a more chemically accurate 6D PES was constructed by Díaz *et al.*[15,39] employing the SRP[40]

approach on DFT. Quantum(Q)/quasi-classical(QC) dynamical calculations had been performed under Born–Oppenheimer static surface (BOSS) approximation to investigate state-resolved dissociative chemisorption probabilities as a function of collision energy for H_2/D_2 (v, j)–Cu(111) systems.

The effect of surface temperature on reaction probability in gas–metal surface collision processes is one of the most fascinating phenomena, which has been explored with different theoretical approaches. For example, AIMD relies on QC trajectories to take into account the surface temperature effect, where the motion of surface atoms is simulated through "on the fly" calculation of forces. In particular, Nattino *et al.*[32] have shown that the use of sufficiently flexible asymmetric sigmoidal generalized logistic function (LGS) for fitting the raw time-of-flight (TOF) spectra provides more accurately fitted experimental reaction probability curves with different saturation values at high collision energies. At 925 K, AIMD calculations demonstrate that theoretical dissociation probability profiles for D_2 (v, j)–Cu(111) systems are close to experimental observations only at low collision energies, but in the high collision energy range, theoretical results are higher in magnitude than the experimental ones. Moreover, the broadening of reaction probability with AIMD is much smaller compared to experimental data.[35]

On the other hand, Wijzenbroek and Somers[30] constructed a static corrugation model (SCM) for dissociation of $H_2/D_2(v, j)$ on Cu(111). The SCM incorporates surface temperature effects by considering thermal expansion and thermal displacements of surface atoms[41] within a vibrational sudden approximation for the dynamics, which are then carried out based on an effectively six-dimensional PES. The resulting QC dynamics has been compared with BOSS and AIMD methods and experimental data.[30] Furthermore, Spiering, Wijzenbroek, and Somers[31] extended the original SCM by including effective three-body interactions and a corrected surface stretching scheme and fitting the model to additional DFT data for chemisorption of D_2 on Cu(111).

In the last few years, construction of chemically accurate high-dimensional neural network potentials (HD-NNPs)[42–47] for various important gas–metal collision processes [e.g., CO_2–Ni(100)/Pt(111),[48–50] NO–Au(111)[51]] has been progressed extensively to overcome the bottleneck of the expensive AIMD method. Such a neural network based approach allows for accurate calculation of reaction probabilities even with very low magnitude (10^{-5}–10^{-4}) for highly activated chemisorption reactions, N_2 + Ru(0001)[52] and CHD_3 + Cu(111).[53] Recently, Zhu *et al.*[54] reported a universal highly transferable PES by employing a newly developed embedded atom neural network (EANN)[55] approach for dissociative chemisorption of H_2 on multiple low-index copper surfaces [Cu(111)/Cu(100)/Cu(110)]. The novel EANN PES allows us to determine quantitative surface temperature (T_s) dependent barrier distributions and, thereby, enables to explore the crucial role of the thermal expansion effect. However, currently, to the best of our knowledge, although 6D QD reaction probabilities were estimated by employing a direct reactive flux method on HD-NNPs[54,56–60] for various systems, QD calculations have not been attempted so far on HD-NNPs to obtain converged inelastic scattering and diffraction probabilities. It remains to be seen if currently available implementations of the HD-NN codes are fast enough to be able to do this with the same accuracy as traditional corrugation reducing procedure[61] (CRP) PESs[30,31,41,62–65] have shown to offer in numerous cases.

Although several first-principles-based theoretical attempts have been made to unveil the effect of surface temperature and its connections to surface vibrations and electronic excitations on molecule–surface scattering processes, the theoretical outcomes are still far away from the actual experimental observations. The following types of broad theoretical approaches have been implemented in the dynamical calculations including the surface mode(s) to account for surface temperature effects: (a) A single or few surface oscillator (SO)[10,18–21,66–69] models have been adapted to construct the Hamiltonians for H_2–Cu(1nn)/Si(100) systems. In addition, theoretical approaches have been improved by considering modified surface oscillator (MSO) models.[20,67] (b) Nave and Jackson investigated[11–13,70] the role of lattice motion[16] and reconstruction for CH_4 dissociation on a Ni(111) plane on a 4D PES at various temperatures within the harmonic approximation. (c) Adhikari and co-workers[25–29] have carried out 4D ⊗ 2D and 6D QD for H_2/D_2 (v, j)–Cu(1nn)/Ni(100) systems by employing the Time Dependent Discrete Variable Representation (TDDVR)-methodology[27,29,71,72] on a more realistic many oscillator[14,25–29] model mimicking a specific plane (1nn) of a metal surface [Cu(1nn)/Ni(100)]. In these approaches, the effective Hamiltonian has been formulated under the mean-field[26–29,71,73] approximation assuming weak coupling among molecular degrees of freedom (DOFs) and surface modes. The vibrational frequencies are computed from a metal–metal Embedded Diatomics in Molecules (EDIM)-fitted[74] potential, while their distributions at the specific temperature are incorporated through the Bose–Einstein (BE) or Maxwell–Boltzmann (MB) probability factor. Although the reaction probabilities obtained from these 6D QD calculations could show up broadening[25–29] as compared to experimental observations at higher surface temperatures (T_s = 1000 K), the sigmoid nature and the appropriate inflection point of the experimental fitted curves[33] are absent in the theoretical ones.

In this work, the surface temperature effect on the transition/reaction probability of the $H_2(v = 0, j = 0)$–Cu(111) system has been investigated more critically by combining a first-principles-based many oscillator model[14,25–29] with a chemically accurate PES from the SCM[30] relying on a mean-field approximation. We have reformulated an effective Hamiltonian by considering the solutions of the linearly forced harmonic oscillator (LFHO),[75] where the surface temperature has been incorporated by taking into account the BE or MB probability factors for the initial state distribution of those modes. The surface mode frequency spectrum and displacement vectors are modeled by a cluster approximation, where the interaction between the copper atoms is described by different potentials. The interaction potential between molecular (H_2) DOFs and surface [Cu(111)] modes and its first derivatives are obtained from the SCM potential. The scattering calculations (6D) have been carried out with the split operator (SPO)-DVR QD code[76] to obtain transition and reaction probabilities of H_2 $(v = 0, j = 0)$ on the Cu(111) surface. Finally, we show reaction and vibrational-state-resolved scattering probabilities in comparison with other theoretical and available experimental results.

II. THEORETICAL BACKGROUND

An effective Hamiltonian has been formulated by invoking a mean-field approach to incorporate the effect of surface vibrational

modes at non-zero surface temperature by introducing the BE probability factors for their initial state distribution. Such an approach allows for time evolution of molecular degrees of freedom (DOFs) ($\{X_k\}$) as well as surface modes ($\{Q\}$) to access all possible configurations arising from their various quantum states, where each subsystem ($\{X_k\}/\{Q\}$) is fully correlated with its all possible configurations. Due to the huge mass difference between the diatom and the metal atoms, the cross correlations among the configurations of different subsystems are neglected by assuming weak interaction, and thereby, a product type wavefunction is considered as follows:

$$\Psi(x, y, z, X, Y, Z, t) \cdot \Phi_{\text{vib}}(\{Q\}, t). \tag{1}$$

The diatomic molecule has six DOFs denoted (x, y, z, X, Y, Z). Here, the Cartesian coordinates x, y, z represent the molecular vector $\mathbf{R} = (R, \theta, \phi)$, and X, Y, Z are the center of mass of the diatom with respect to the Cu surface such that the top layer of the Cu atoms corresponds to $Z = 0$. Surface vibrational wavefunctions [$\Phi_{\text{vib}}(\{Q\})$] and their concomitant frequencies ($\{\omega_k\}$) are modeled by the 87 (=3 $*$ 31 − 6) normal modes of a Cu_{31} cluster that has been cut out of the topmost three layers of the Cu(111) surface. The interaction between the copper atoms is described by the SRP48 DFT functional as implemented in Vienna *Ab initio* Simulation Package DFT code[15] (VASP-SRP48), the embedded-atom method (EAM) potential originally developed by Folies, Baskes, and Daw (FBD),[77] and a potential based on the Embedded Diatomics in Molecules (EDIM) model.[74] Further computational details about these frequency calculations are described in the supplementary material. Figure 1 shows the three different resulting frequency spectra.

The product-type wavefunction [Eq. (1)] leads to the following form of time and temperature dependent effective Hamiltonian:

$$\begin{aligned}\widehat{H}(x, y, z, X, Y, Z, t, T_s) &= -\frac{\hbar^2}{2\mu}\left(\frac{\partial^2}{\partial x^2} + \frac{\partial^2}{\partial y^2} + \frac{\partial^2}{\partial z^2}\right) - \frac{\hbar^2}{2M}\left(\frac{\partial^2}{\partial X^2} + \frac{\partial^2}{\partial Y^2} + \frac{\partial^2}{\partial Z^2}\right) \\ &\quad + V_0(x, y, z, X, Y, Z) + V_{\text{eff}}(x, y, z, X, Y, Z, t, T_s),\end{aligned} \tag{2}$$

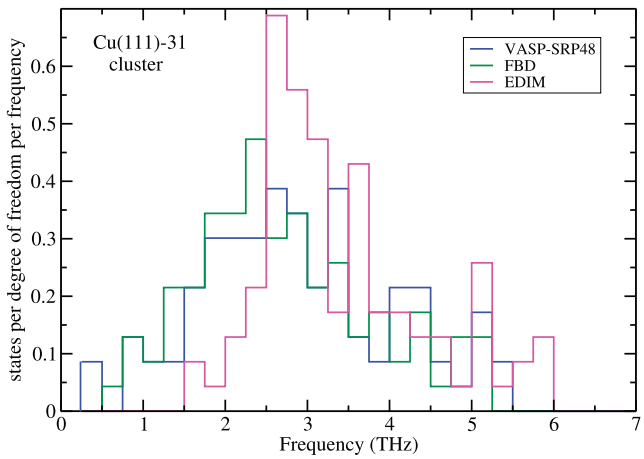

FIG. 1. Frequency distributions of the Cu_{31} cluster models as described in the text, calculated with the VASP-SRP48, FBD, and EDIM potentials.

where μ and M are the reduced and the total mass of the diatom, respectively. $V_0(x, y, z, X, Y, Z)$ is the rigid surface (RS)–molecule interaction potential known as the BOSS PES[15,39] describing the situation of ideal static lattice (i.e., excluding the effect of surface DOFs), where $V_{\text{eff}}(x, y, z, X, Y, Z, t, T_s)$ is the effective Hartree potential due to the surface mode coupling with molecular DOFs.

It is worth mentioning that although the dynamics of the molecule is characterized by a single wavepacket evolution (apparently pure state representation), the effective Hartree potential V_{eff} arising from the coupling of molecular DOFs and surface modes (bath) is constructed by taking into account an ensemble average of different pure state configurations (i.e., mixed state situation) through the employment of the MB/BE probability factor, and consequently, the surface temperature is introduced into the effective Hamiltonian parametrically. Therefore, such product type of Hartree wavefunction description could simulate the molecular beam experimental situation, where the molecule and surface initially are not in thermal equilibrium with each other.

A. Formulation of the effective Hartree potential (V_{eff})

The effective Hartree potential averaged over the initial state $\{n_0\}$ distribution of vibrational modes is defined as (see Appendix A)

$$V_{\text{eff}}(x, y, z, X, Y, Z, t, T_s) = \langle V \rangle(t, T_s) = \sum_{\{n_0\}} p_{\{n_0\}} \langle V \rangle_{\{n_0\}}, \tag{3}$$

where the initial states are averaged out by considering the Bose–Einstein (BE) or Maxwell–Boltzmann (MB) distribution over various surface modes (k),

$$p_{\{n_0\}} = \prod_{k=1}^{M} p_{n_k^0}^{(k)}. \tag{4}$$

The initial state $\{n_0\}$ dependent Hartree potential due to the interaction potential (V_I) between gas molecular DOFs and surface modes is expressed as

$$\begin{aligned}\langle V \rangle_{\{n_0\}} &= \langle \Psi(t) | V_I | \Psi(t) \rangle \\ &= \sum_{\{n'\}} \sum_{\{n\}} \alpha^*_{\{n'\} \leftarrow \{n_0\}}(t)\, \alpha_{\{n\} \leftarrow \{n_0\}}(t) \langle \{n'\} | V_I | \{n\} \rangle,\end{aligned} \tag{5}$$

where $\{n\}$ and $\{n'\}$ are the all possible quantum states accessible by the vibrational modes. The amplitudes $\alpha_{\{n\}}(t)$ originating from the initial state $\{n_0\}$ to final ones $\{n\}$ under the evolution operator, $U(t, t_0)$, due to the molecule–surface interaction are defined as

$$\alpha_{\{n\} \leftarrow \{n_0\}}(t) = \langle \{n\} | U | \{n_0\} \rangle. \tag{6}$$

While averaging over all possible final quantum states ($\{n\}$ and $\{n'\}$) in Eq. (5), the interaction potential (V_I) between molecular DOFs and surface modes needs to be expanded in terms of the normal mode coordinate (Q_k). Furthermore, these coordinates are expressed in terms of boson creation ($b_k^\dagger$)/annihilation (b_k) operators such as $Q_k = A_k(b_k^\dagger + b_k)$ and $A_k = \sqrt{\hbar/2\omega_k}$, and thereby, the interaction potential considering only up to first order terms takes the following form:

$$V_I = V_0 + \sum_{k=1}^{M} \lambda_k A_k (b_k F_k^- + b_k^+ F_k^+) V_{k,1}, \tag{7}$$

where $F_k^- = \exp(-i\omega_k t)$, $F_k^+ = (F_k^-)^*$, and $V_{k,1} = \partial V_I/\partial Q_k|_{eq}$.

Finally, the first derivative of the interaction potential ($V_{k,1}$) with respect to the normal mode (Q_k) is evaluated by employing the chain rule of differentiation with respect to the metal atomic position $\left(\frac{\partial V_{a\alpha}^{\text{Cu-H}}}{\partial X_{\alpha i}}\right)$, as follows:

$$\begin{aligned} V_{k,1} &= \left(\frac{\partial V_I}{\partial Q_k}\right) = \sum_{a\alpha} \frac{\partial (V_{a\alpha}^{\text{Cu-H}}(r_{a\alpha}) - V_{a\alpha}^{\text{Cu-H}}(r_{a\alpha}^{\text{id}}))}{\partial Q_k} \\ &= \sum_{a\alpha i}\left[\frac{\partial V_{a\alpha}^{\text{Cu-H}}(r_{a\alpha})}{\partial X_{\alpha i}} - \frac{\partial V_{a\alpha}^{\text{Cu-H}}(r_{a\alpha}^{\text{id}})}{\partial X_{\alpha i}}\right]\cdot\frac{\partial X_{\alpha i}}{\partial Q_k} \\ &= \sum_{a\alpha i} m_\alpha^{-1/2}\left[\frac{\partial V_{a\alpha}^{\text{Cu-H}}(r_{a\alpha})}{\partial X_{\alpha i}} - \frac{\partial V_{a\alpha}^{\text{Cu-H}}(r_{a\alpha}^{\text{id}})}{\partial X_{\alpha i}}\right] T_{\alpha i;k}, \end{aligned} \tag{8}$$

where the following equation is used to calculate $\frac{\partial X_{\alpha i}}{\partial Q_k}$:

$$X_{\alpha i} - X_{\alpha i}^{\text{id}} = m_\alpha^{-1/2}\sum_k T_{\alpha i;k} Q_k, \tag{9}$$

and the derivative of the SCM potential[30] $\left(\frac{\partial V_{a\alpha}^{\text{Cu-H}}}{\partial X_{\alpha i}}\right)$ is shown in Appendix B.

The indices α, a, and k denote the metal atom, gas atom, and normal mode, respectively, where $\alpha = 1, 2, \ldots, N$, $N = 31$ (number of metal atoms), $a = 1$, 2, and $k = 7, 8, \ldots, 3N$, where the first six modes are the translational and rotational DOFs. $X_{\alpha i}$ is the position of a metal atom, where $X_{\alpha i}^{\text{id}}$ is its equilibrium position for a specific degree of freedom, i. Q_k is the normal mode coordinate, m_α is the mass of the surface atom, and $T_{\alpha i;k}$ is the transformation matrix between local (αi) and normal (k) modes. On the other hand, $r_{a\alpha}$ is the distance between each metal atom (α) and gas atom (a). $V_{a\alpha}^{\text{Cu-H}}(r_{a\alpha})$ and $V_{a\alpha}^{\text{Cu-H}}(r_{a\alpha}^{\text{id}})$ are the gas–metal interaction potentials due to displaced and ideal positions of the metal atoms, respectively.

Inserting Eq. (7) in Eq. (5), and then in Eq. (3) for the BE or MB cases, we arrive at the following compact form of the effective Hartree potential:

$$\begin{aligned} &V_{\text{eff}}^{\text{BE}}(x, y, z, X, Y, Z, t, T_s) \\ &= \frac{1}{N_{\text{BE}}}\left[\sum_{k=7}^{3N}\lambda_k\frac{1}{\omega_k^2}V_{k,1}^2[\cos\omega_k(t-t_0)-1]\sum_{q=1}^{\infty}\frac{z_k^{q/2}}{(1-z_k^q)}\right], \end{aligned} \tag{10}$$

where $N_{\text{BE}} = \sum_k \sum_{n_k^0=0}^{\infty} \frac{1}{\exp[\hbar\omega_k(n_k^0+\frac{1}{2})\beta]-1}$ is the normalization of the Bose–Einstein probability factor for vibrational modes. On the contrary, in case of the Maxwell–Boltzmann probability factor, the form of the effective Hartree potential will be

$$\begin{aligned} &V_{\text{eff}}^{\text{MB}}(x, y, z, X, Y, Z, t, T_s) \\ &= \frac{1}{N_{\text{MB}}}\left[\sum_{k=7}^{3N}\lambda_k\frac{1}{\omega_k^2}V_{k,1}^2[\cos\omega_k(t-t_0)-1]\frac{z_k^{1/2}}{(1-z_k)}\right], \end{aligned} \tag{11}$$

with $N_{\text{MB}} = \sum_k \sum_{n_k^0=0}^{\infty} \exp\left[-\hbar\omega_k\left(n_k^0+\frac{1}{2}\right)\beta\right]$. The associated sign (− or +) of the first derivative of the interaction potential is denoted λ_k.

Some important aspects of the effective Hamiltonian are as follows: (a) For both the BE and MB cases, the frequency (ω_k) of the surface modes appears multiple times in the time and temperature dependent terms of the effective potential. Therefore, the frequency spectrum (see Fig. 1) calculated by different approaches (VASP-SRP48, FBD, and EDIM) from the surface atom interaction potential is expected to play a crucial role in the reaction and scattering probabilities. (b) The functional form of the temperature dependent term of the effective potential in terms of the partition function differs for the BE ($\sum_{q=1}^{\infty}\frac{z_k^{q/2}}{(1-z_k^q)}$) and MB [$\frac{z_k^{1/2}}{(1-z_k)}$] cases, and thereby, their contributions would be different to the broadening of reaction probabilities at a particular temperature. (c) The magnitude and the occurrence of the first derivative of the interaction potential ($V_{k,1}$) should have a role in the reaction probability (see Fig. 6). (d) For the specific surface mode frequency (ω_k) and temperature (T_s), the contribution of the Hartree potential is modulated as a function of time of the collision process.

B. Mean-field approach and sudden approximation

The theoretical description of the molecular DOF–surface mode interaction and the dynamical outcomes of the gas–metal surface scattering process are described using the mean-field approach and sudden approximation as follows.

(a) The explicit correlations between molecular DOFs and surface mode vibrations are neglected in both the approaches either by sampling the lattice vibration (Q) using MB distribution (sudden approximation[11–13,16,70]) or by employing a Hartree product type of wavefunction (mean-field approach[26–29,71,73]) through the construction of the effective potential. In both cases, only the effective contribution of the surface mode vibrations at the particular surface temperature is taken into account on the motion of the incoming molecule. (b) In the mean-field treatment, the effective potential has been constructed by including all possible initial state configuration ($\{n_0\}$) through the employment of MB/BE distribution by considering all the vibrational states for each surface mode (k). Such effective potential changes with time during the course of the collision process due to surface mode excitations at the particular temperature. Moreover, time dependence of the effective potential also varies for different surface temperatures and kinetic energies (KEs) of the diatom. Therefore, instantaneous effects of molecule–lattice atom interactions are incorporated in the effective potential implicitly within the mean-field approach. On the other hand, such responses of the lattice atoms (e.g., instant puckering) had been considered in sudden approximation treatment by performing scattering calculations on different sampled (classically) points ($\{Q\}$) of the lattice vibration (Q) at the given surface temperature. (c) Ensemble average of scattering probabilities obtained from the sudden approximation over infinitely distinct sampled values of a large configuration space and the scattering profile resulting from the mean-field approach by taking the time average over infinitely different effective potentials arising from all possible configuration could have comparable levels of approximations due to the neglect of higher order correlations between molecular DOFs and surface modes. The applicability of both approaches could be validated only through the implementation on specific system(s).

C. Computational details for the effective Hartree potential

The expression of the effective Hartree potential contains the derivatives of the interaction potential ($V_{k,1} = \frac{\partial V_1}{\partial Q_k}$), frequency ($\omega_k$) of surface modes ($Q_k$), and time $[[\cos\omega_k(t-t_0)-1]]$ and temperature $[\sum_{q=1}^{\infty}\frac{z_k^{q/2}}{(1-z_k^q)}$ for BE, $\frac{z_k^{1/2}}{(1-z_k)}$ for MB] dependent terms [see Eqs. (10) and (11)]. The derivatives of the interaction potential with respect to the normal modes ($V_{k,1} = \frac{\partial V_1}{\partial Q_k}$) have been computed with the chemically accurate SCM[30] potential, where the transformation matrix ($T_{\alpha i;k}$) between local ($X_{\alpha i}$) and normal (Q_k) modes is being employed. The frequency spectrum ($\{\omega_k\}$) and displacement vector ($T_{\alpha i;k}$) of surface modes (Q_k) have been evaluated by using the VASP-SRP48, FBD, or EDIM surface atom interaction potentials. With such an effective Hamiltonian, we perform 6D QD for H_2 on Cu(111) starting with the hydrogen molecule in its rovibrational ground state ($v = 0$, $j = 0$) using the SPO-DVR code.[76] The parameters of the SRO-DVR code are given in Sec. 2 of the supplementary material. We calculate reaction and scattering probabilities for various surface temperatures (T_s = 1 K, 120 K, 300 K, 600 K, and 925 K).

III. RESULTS

For the surface temperature of 120 K, using VASP-SRP48 calculated normal mode frequencies, the convergence profiles of reaction probability as a function of the basis set as well as the cutoff on the derivative of the interaction potential ($V_{k,1}^2$) are demonstrated in Figs. 2(a) and 2(b), respectively. On the other hand, for a 925 K situation, the convergence test of reaction probability profiles is performed with the same basis set functions (lower and higher bases) as used in the 120 K case [see Fig. 2(c)]. It is worth mentioning that performing QD calculations with a further larger basis set is computationally very expensive. There are two important things to note from these figures: (a) The dependence of reaction probability with lower, intermediate, and higher basis sets for 120 K and with lower and higher ones for 925 K is minimum except at higher collision energies for lower basis. (b) The different values (1.0×10^{-11}, 5.0×10^{-12}, and 1.0×10^{-12}) of cutoff on the derivative of the interaction potential ($V_{k,1}^2$) do not show any effect for the 120 K case. Moreover, it has been observed that if the magnitude of the cutoff does not show any effect within the cutoff on $V_{k,1}^2 \leq 1 \times 10^{-12}$, there is no effect on further lowering of the cutoff, which has been numerically verified. In contrast, at 925 K surface temperature, the cutoff on $V_{k,1}^2$ is imposed for the condition $V_{k,1}^2 \leq 1.0 \times 10^{-11}$.

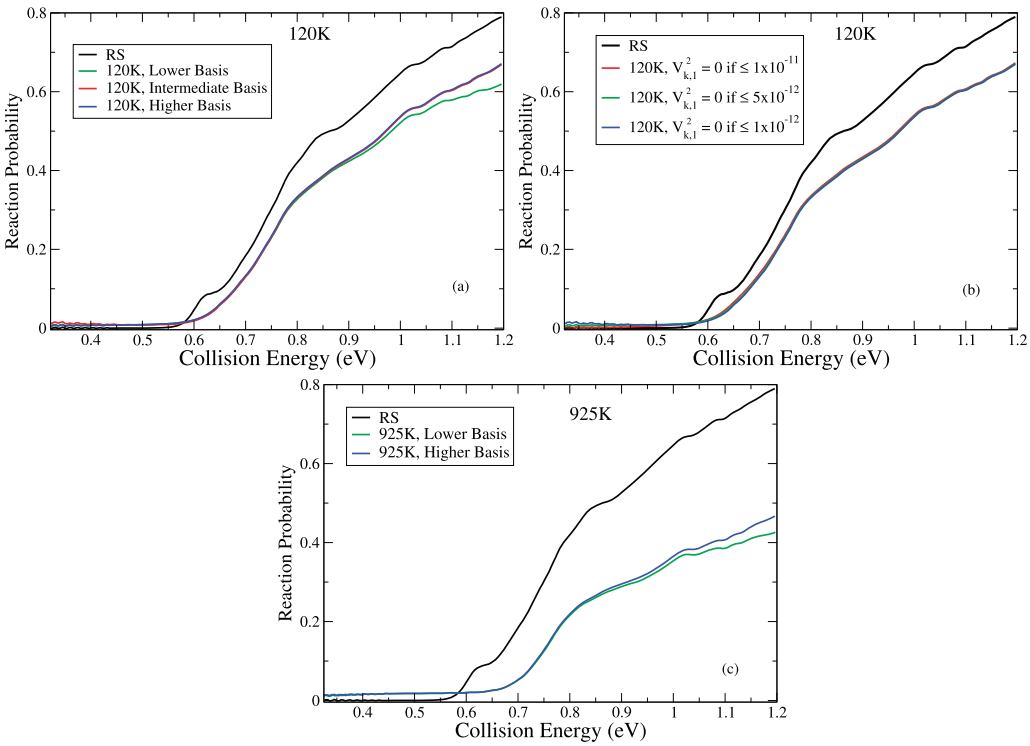

FIG. 2. Convergence of the reaction probability for H_2 on Cu(111) with the VASP-SRP48 calculated normal mode frequencies as a function of the (a) basis set with lower (X = 18, Y = 18, Z = 140, R = 64, j_{max} = 12, and $m_{j max}$ = 6), intermediate (X = 18, Y = 18, Z = 180, R = 64, j_{max} = 20, and $m_{j max}$ = 10), and higher (X = 18, Y = 18, Z = 180, R = 64, j_{max} = 24, and $m_{j max}$ = 12) bases for 120 K; (b) cut-off by setting $V_{k,1}^2$ equal to zero if its magnitude is $\leq 1.0 \times 10^{-11}$, $\leq 5.0 \times 10^{-12}$, and $\leq 1.0 \times 10^{-12}$, respectively, at 120 K; (c) basis set with lower (X = 18, Y = 18, Z = 140, R = 64, j_{max} = 12, and $m_{j max}$ = 6) and higher (X = 18, Y = 18, Z = 180, R = 64, j_{max} = 24, and $m_{j max}$ = 12) bases for 925 K surface temperature by imposing the cutoff condition $0 = V_{k,1}^2 \leq 1.0 \times 10^{-11}$.

A. Effect of quantum vs classical initial vibrational state populations on the reaction probability

In Figs. 3(a), 3(b), 4(a), and 4(b), we present the contribution of the normalized probability factor [see Eq. (A8) in Appendix A] due to the BE and MB statistics as a function of the frequency number calculated from the EDIM and VASP-SRP48/FBD potentials at 120 K and 925 K surface temperatures, respectively. In case of the EDIM normal modes, Figs. 3(a) and 4(a) depict the magnitudes of the normalized probability factor over the entire range of vibrational frequencies at 120 K and 925 K, where their values are quite low and close to each other for both the MB and BE statistics. As a result, the EDIM frequencies do not show any broadening [see Fig. 3(c)] or have an almost negligible effect on the reaction probabilities [see Fig. 4(c)] with either the BE or the MB statistics both at the surface temperature of 120 K and 925 K. On the other hand, for the VASP-SRP48/FBD cases, Figs. 3(b) and 4(b) depict two important features: (i) the BE and MB probability factors appear steeply higher in magnitude in the lower frequency regime compared to those probability factors in the EDIM; (ii) the normalized probability factor for the BE distribution is much higher in magnitude than that of the MB statistics. Although the profiles of the normalized probability factor for the BE and MB statistics are reversed by small magnitudes in the higher frequency range, their contributions to the reaction probability are expected to be very low at either 120 K or 925 K. Therefore, the origin of substantial broadening of reaction probabilities [see Figs. 3(d) and 4(d)] at 120 K and 925 K surface temperatures with the BE statistics compared to the MB one in case of VASP-SRP48/FBD could be attributed to the existence of sufficiently higher magnitude of the normalized probability factor in the lower frequency range.

While exploring the effect of the normal modes on the Hartree potential, we employ a cross combination of frequencies and displacement vectors obtained from the various approaches (VASP-SRP48, FBD, and EDIM) to construct a Hartree potential only with the BE probability factor and, then, to calculate reaction probabilities with such potential at 120 K. In Fig. 5(a), when the EDIM calculated frequencies are used along with the VASP-SRP48, FBD, and EDIM calculated displacement vectors, the broadening of the reaction probability is essentially absent. On the

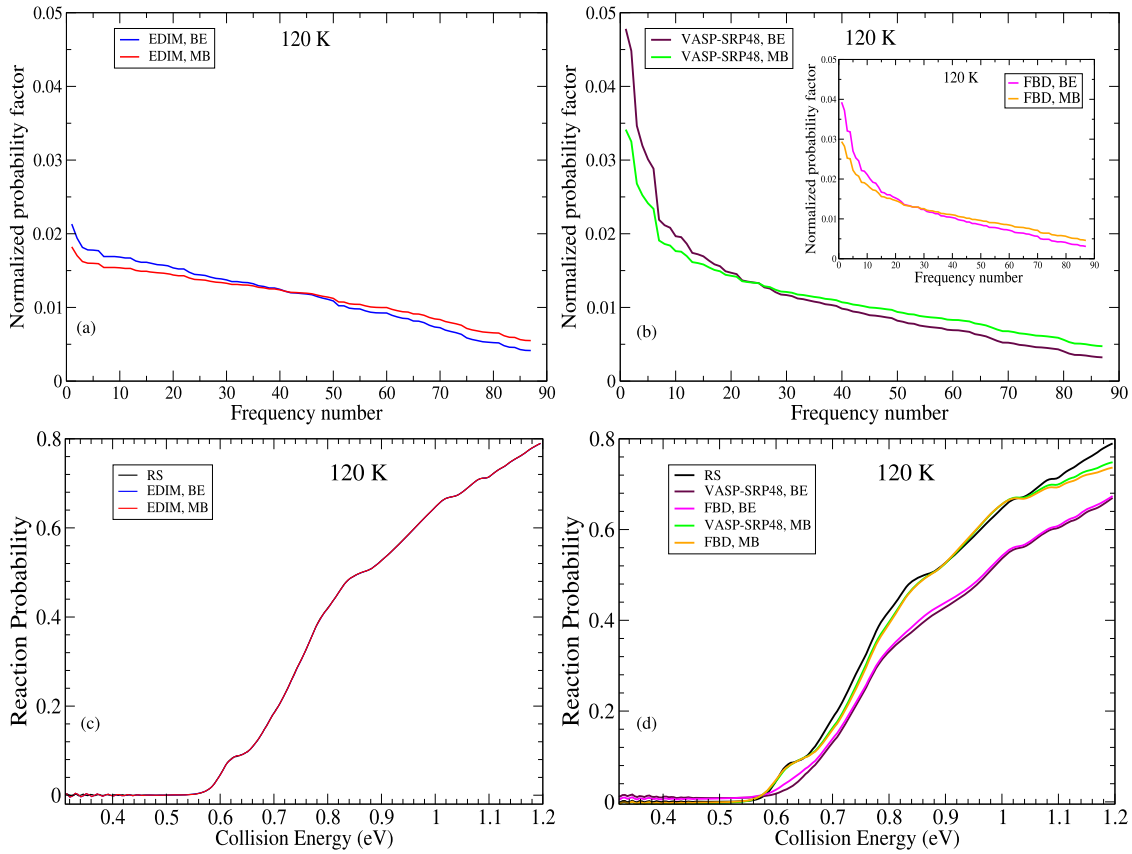

FIG. 3. Normalized probability factor as a function of the frequency number with the BE and the MB distribution at 120 K for (a) the EDIM normal mode frequencies and (b) the VASP-SRP48/FBD normal mode frequencies. Reaction probabilities for H_2 on Cu(111) calculated based on the Hartree potential constructed with (c) the EDIM and (d) the VASP-SRP48/FBD calculated normal mode frequencies along with the MB and the BE probability factor at 120 K surface temperature.

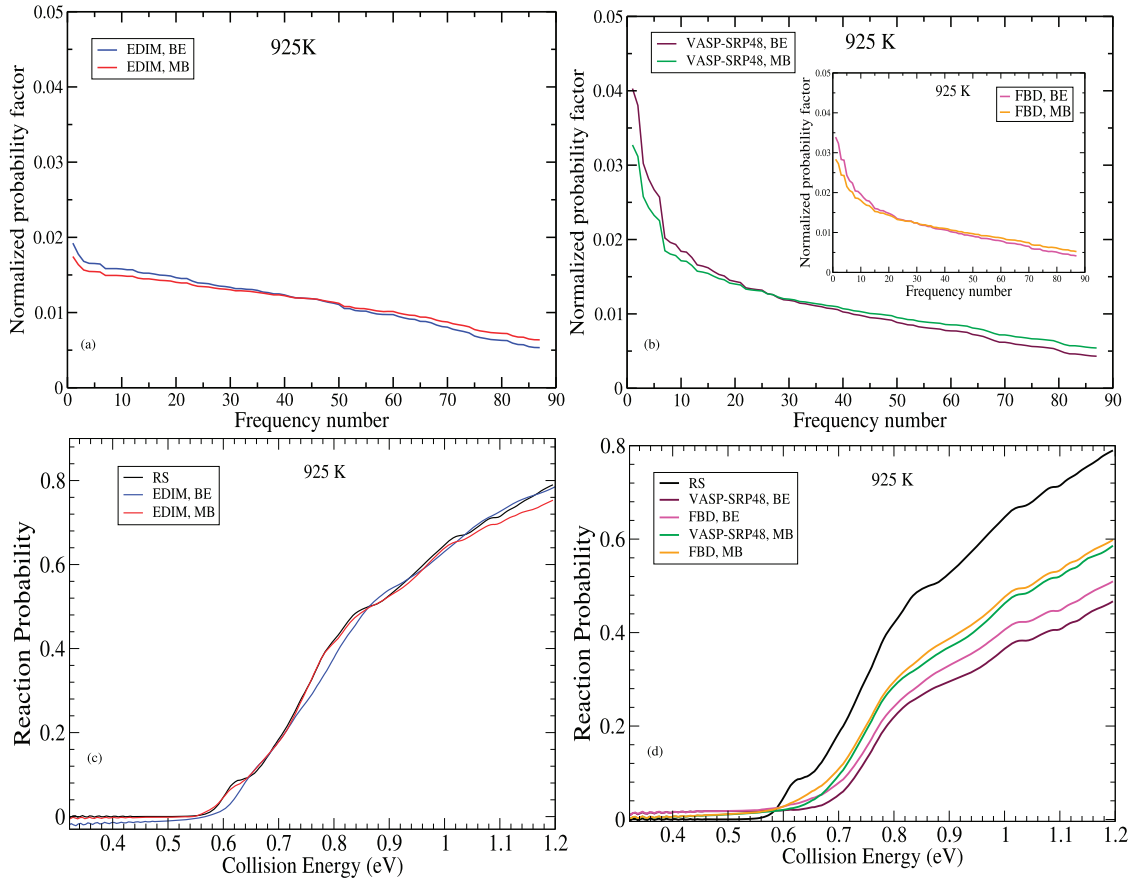

FIG. 4. The same as Figs. 3(a)–3(d), but for the surface temperature of 925 K.

other hand, Figs. 5(b) and 5(c) show that when the VASP-SRP48 or FBD calculated normal mode frequencies are used along with the VASP-SRP48, FBD, and EDIM calculated displacement vectors, the broadening of the reaction probability is substantial. Therefore, the quantization of the surface modes [see Figs. 5(a)–5(c)] vis-à-vis the distribution [see Figs. 3(c), 3(d), 4(c), and 4(d)] of normal modes with the BE probability factor is the key element for the origin of broadening.

B. Influence of surface mode excitation on the reaction probability

While constructing the Hartree potential, we need to calculate a crucially important quantity known as surface mode forcing $[\left(\frac{V_{k,1}}{\omega_k}\right)^2]$, which is an average measure of surface mode excitation due to the coupling with the incoming molecule. The contribution of $\left(\frac{V_{k,1}}{\omega_k}\right)^2$ $(=N^{oc}_{V_{k,1}})$ to the effective Hartree potential affecting the scattering process vis-à-vis reaction probability is discussed at this junction. Figures 6(a) and 6(b) display the profiles of $N^{oc}_{V_{k,1}}$ over each specific magnitude as a function of the normal mode frequency for the EDIM and VASP-SRP48 cases. The distribution of $N^{oc}_{V_{k,1}}$ over the different magnitudes for a specific vibrational mode (k) has been fitted with a Gaussian function $[A\exp(-(\frac{x-x_0}{\sigma})^2)]$. Figures 6(c) and 6(d) depict the variations of the amplitude (A)/mean amplitude $(\langle A\rangle)$ and the width (σ)/mean width $(\langle\sigma\rangle)$ of the fitted Gaussians for the EDIM and VASP-SRP48 cases, respectively, as a function of the normal mode (k). Since widths (σ)/mean widths $(\langle\sigma\rangle)$ show an opposite trend compared to amplitudes (A)/mean amplitudes $(\langle A\rangle)$ as a function of normal modes, it may not be easy to interpret the overall contribution of $N^{oc}_{V_{k,1}}$ to the reaction probability. On the contrary, those profiles $(\sigma, \langle\sigma\rangle, A, \langle A\rangle)$ for VASP-SRP48 are steeply changing compared to the EDIM case, and thereby, the VASP-SRP48 frequency spectrum affects the scattering process significantly leading to higher broadening as depicted in Figs. 3(c), 3(d), 4(c), 4(d), 5(a), and 5(b).

C. Temperature-dependent reaction and state-to-state scattering probabilities

Since the VASP-SRP48 and FBD calculated frequencies and displacement vectors show up substantial broadening (Figs. 3–5) over EDIM calculated ones, we choose VASP-SRP48 normal mode

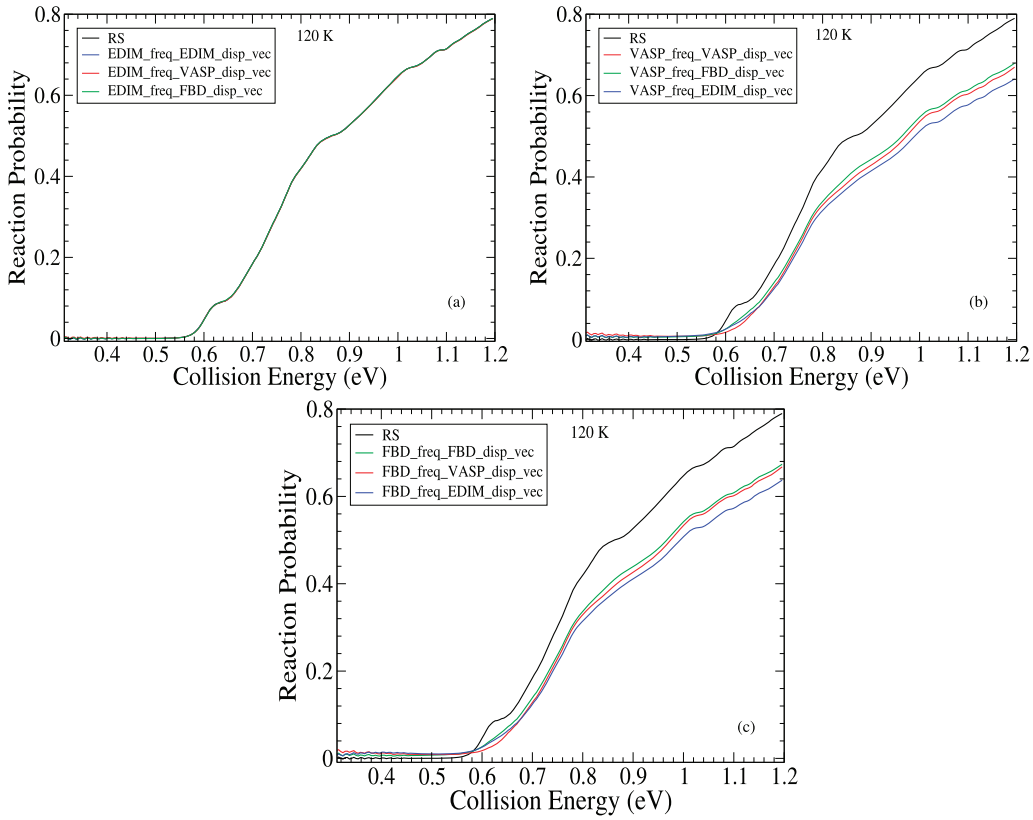

FIG. 5. Reaction probabilities for H_2 on Cu(111) calculated based on the Hartree potential at 120 K surface temperature constructed with the (a) EDIM calculated normal mode frequencies along with the EDIM, VASP-SRP48, and FBD calculated displacement vectors; (b) VASP-SRP48 calculated normal mode frequencies along with the VASP-SRP48, FBD, and EDIM calculated displacement vectors; (c) FBD calculated normal mode frequencies along with the FBD, VASP-SRP48, and EDIM calculated displacement vectors.

frequencies/displacement vectors to construct the Hartree potential and calculate reaction and state-to-state scattering probabilities at various surface temperatures. For 1 K, 120 K, and 300 K surface temperatures, the dynamics are performed by considering the effective Hartree potential constructed with the VASP-SRP48 calculated normal mode frequencies without imposing any approximation, namely, the cutoff on $V^2_{k,1}$ and the converged reaction probabilities are obtained as depicted in Fig. 7. On the other hand, for 600 K and 925 K surface temperatures, it appears (numerically) that we need to impose a cutoff on the derivative of the interaction potential ($V^2_{k,1}$) to get converged reaction probabilities (also see Fig. 7), where, for each mode (k), $V^2_{k,1}$ is set to zero if the quantity ($V^2_{k,1}$) is $\leq 5 \times 10^{-12}$ and $\leq 1 \times 10^{-11}$, respectively. There are three points to note: (a) The reaction probability profiles for the RS and the 1 K surface are perfectly merged with each other over the considered range of collision energies (0.3 eV–1.2 eV). (b) The broadening of reaction probabilities increases with the increase in surface temperature, but the rate of broadening with respect to surface temperature is steadily decreasing (see Fig. 7). (c) Moreover, it is evident from the log scale representation of reaction probabilities that QD results are enhanced considerably with the increase in surface temperature in the low kinetic energy domain compared to the RS and 1 K ones. Such enhancement of reaction probabilities (see the inset of Fig. 7) may appear either due to the quantum effect at those surface temperatures or due to the numerical issues associated with the dynamical calculations, where the latter creates unphysical oscillation in QD reaction probabilities as described in Sec. 2 of the supplementary material [2. (*Parameters and details of the 6D QD calculations using SPO-DVR* code[3])].

The inset of Fig. 7 reflects that even though, in the low energy region, our QD probabilities for 1 K, 120 K, and 300 K surface temperatures are first diminished and then increased after passing through minima with the increase in kinetic energy (where the positions of the minima are shifted toward low kinetic energy with the increase in surface temperature from 1 K to 120 K–300 K), such a feature is totally absent for the 600 K and 925 K cases. On the contrary, a similar feature is found experimentally at 923 ± 3 K by Kaufmann *et al.*[37] due to the existence of the unusual slow channel for the dissociation of H_2 on the Cu(111) surface. These trends in 6D QD reaction probabilities at lower temperatures (1 K, 120 K, and 300 K) could arise from the reflection related to the optical potentials or numerical inaccuracy associated with the larger time step in

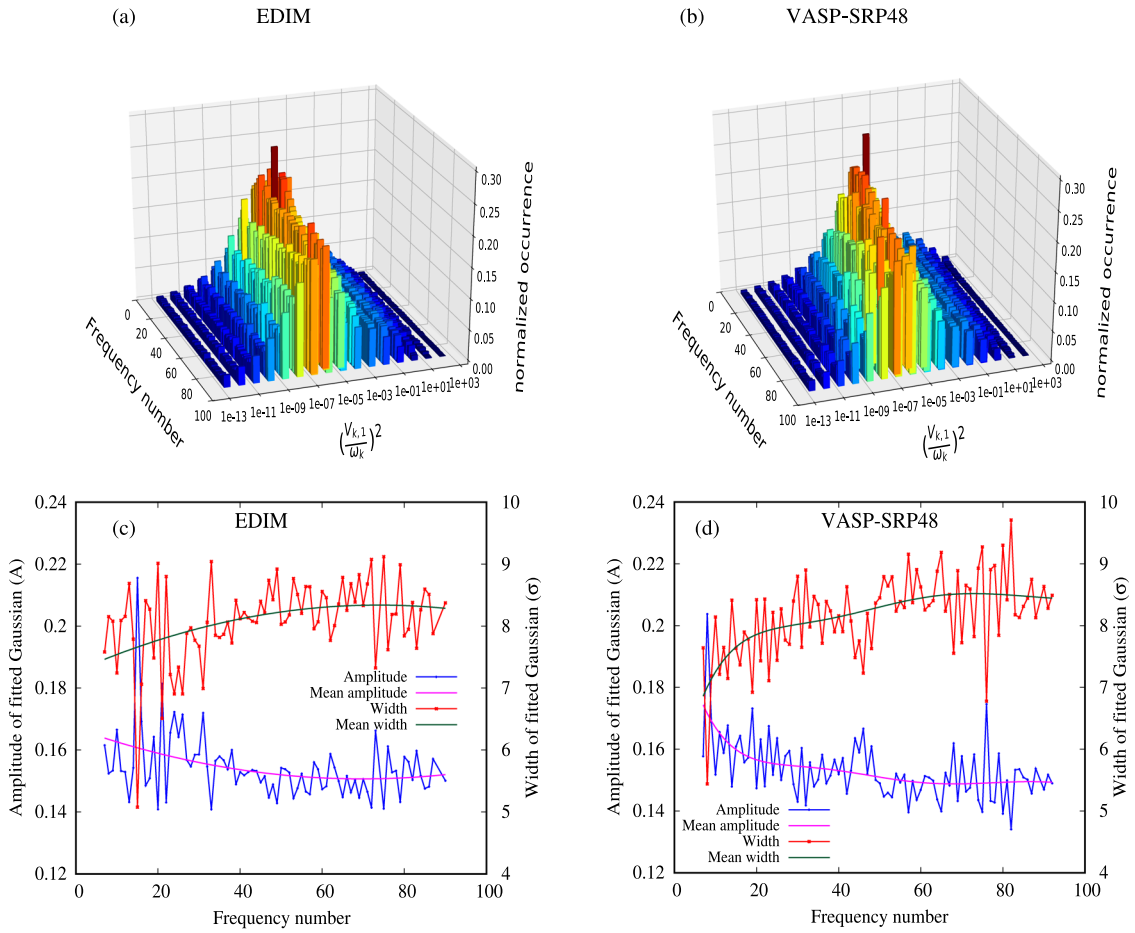

FIG. 6. For the 6D SCM potential, the normalized occurrence of $\left(\frac{V_{k,1}}{\omega_k}\right)^2$ (=$N^{oc}_{V_{k,1}}$) over its various magnitudes and the frequency number (k) calculated from (a) the EDIM and (b) the VASP-SRP48 surface atom interaction potential are shown. For each vibrational mode (k), amplitudes (A)/mean amplitudes ($\langle A \rangle$) and widths (σ)/mean widths ($\langle \sigma \rangle$) of the fitted Gaussian over the different magnitudes of $N^{oc}_{V_{k,1}}$ are depicted as a function of the frequency number (k) in (c) and (d), respectively.

SPO-DVR propagation or total time propagation (or a combination of all the three) while including Hartree potentials for the finite surface temperature situations.

Figure 8 depicts the profile of vibrational state-to-state scattering probabilities for the scattered $H_2(v' = 0, 1)$ molecule employing the effective Hartree potential constructed with the VASP-SRP48 normal mode frequencies as a function of various initial collision energies of the incoming molecule [$H_2(v = 0, j = 0)$] for 1 K, 120 K, 300 K, 600 K, and 925 K surface temperatures. We find both the survival ($v' = 0$) and excitation ($v' = 1$) probabilities are increasing with the increase in surface temperature, thereby leading to a broadening of the reaction probability with the increase in surface temperature (T_s). For the VASP-SRP48 case, the final rotational state distribution is displayed in Figs. 9(a) and 9(b) for the scattered $H_2(v' = 0/1, j')$ as a function of j' at a particular collision energy (1.08 eV) for different surface temperatures. It is evident that transition probabilities attain a maximum value at a particular rotational state (j') for all the temperatures, but the distributions become wider as the temperature increases. Moreover, the effect of temperature on the rotational state resolved transition probabilities is more pronounced in the ground vibrational state ($v' = 0$) compared to the excited state ($v' = 1$).

IV. DISCUSSION

Finally, we compare our QD results for the reaction probabilities at 120 K with other theoretical profiles and for the probabilities at 925 K with both various theoretical and experimental results. Figure 10(a) depicts our QD result along with QC trajectory calculations obtained from the SCM[30] at 120 K surface temperature. On the other hand, in Figure 10(b), a comparison between extracted recombinative desorption experimental[33] data and various theoretical results is shown for 925 K surface temperature. We emphasize that the SCM-QC[30] is based on the same six-dimensional VASP-SRP48 PES and includes thermal displacements of surface atoms within sudden approximation as well as expansion of the lattice at 120 K and 925 K surface temperatures. Figure 10(a) reflects that

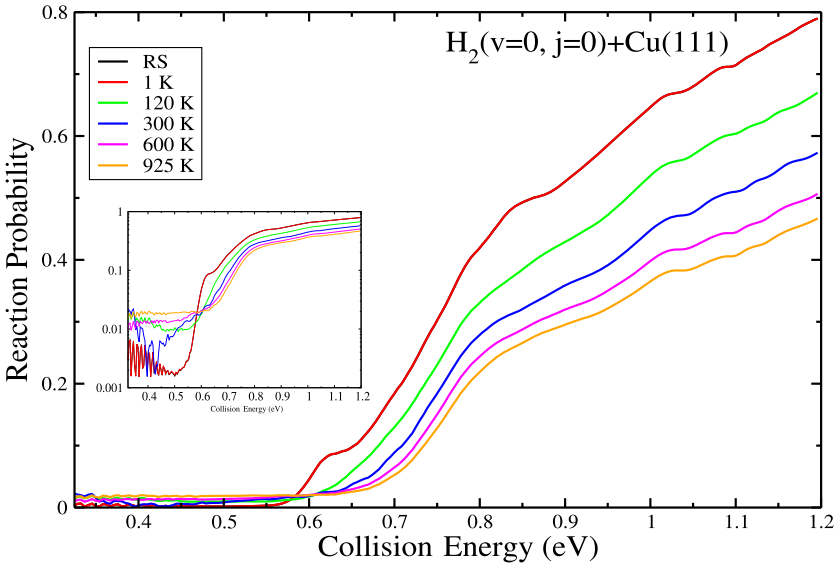

FIG. 7. Reaction probabilities for H_2 on Cu(111) based on the RS and the effective Hartree potential constructed with the VASP-SRP48 calculated normal mode frequencies at 1 K, 120 K, 300 K, 600 K, and 925 K surface temperatures, where, only for 600 K and 925 K, $V^2_{k,1}$ is set to zero if its magnitude is $\lesssim 5.0 \times 10^{-12}$ and $\lesssim 1.0 \times 10^{-11}$, respectively. The reaction probabilities at different surface temperatures are also presented in the log scale as an inset.

our 6D QD-Hartree calculation provides higher reaction probability with respect to the other QC methods at very low collision energy for 120 K surface temperature (also see its inset). Although the unphysical oscillations at 120 K are much smaller compared to the RS and 1 K situations (see the inset of Fig. 7), such enhancement of the QD reaction probabilities with respect to QC ones in the low energy region could emerge from the quantum effect or may be due to the numerical issues associated with the optical potential or larger time step or total time propagation (or a combination of all the three) in SPO-DVR propagation at that temperature. On the other hand, our 6D QD results at lower surface temperature (120 K) agree quite well with other theoretically calculated reaction probabilities close to and beyond the threshold energy. In contrast, for higher surface temperature (925 K), it is evident from Fig. 10(b) that, over the moderate collision energies, our results deviate from the experimental and other theoretical results, which indicates the limitation of the mean-field approach at higher temperatures. At the same time, despite the fact that the high energy domain of the experimental reaction probability profile is disputable (see Sec. 1 of the supplementary material) for H_2 scattering from Cu(111) in the rovibrational ground state, reaction probabilities obtained by incorporating a chemically accurate SCM potential within the mean-field approach are more

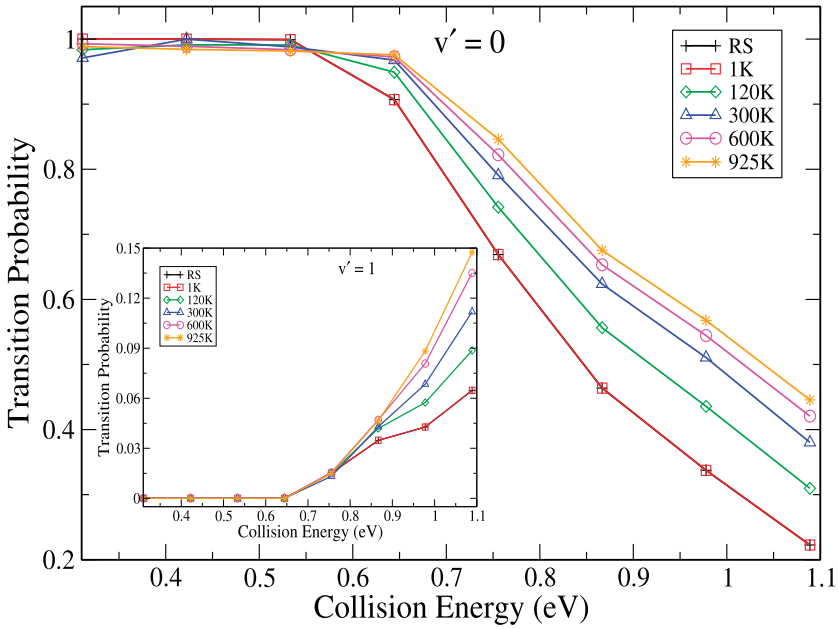

FIG. 8. State-to-state transition probabilities for $H_2(v = 0, j = 0)$/Cu(111) $\rightarrow$ $H_2(v' = 0, 1)$/Cu(111) on the RS and on the Hartree potential constructed with the VASP-SRP48 calculated normal mode frequencies at 1 K, 120 K, 300 K, 600 K, and 925 K surface temperatures.

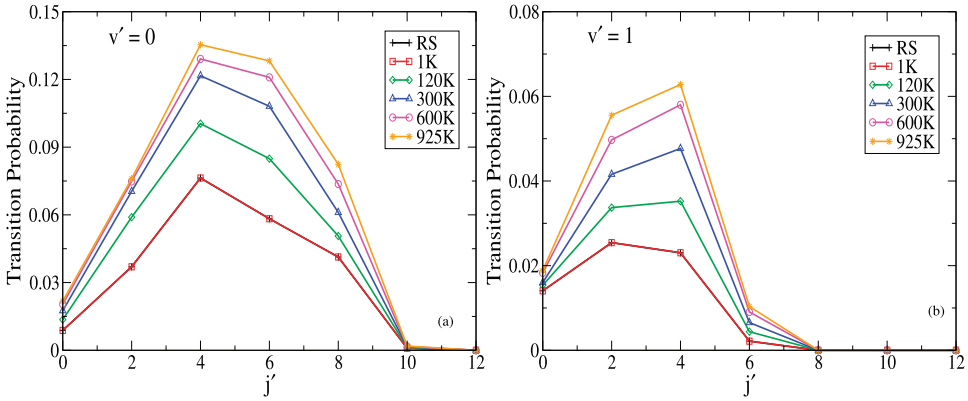

FIG. 9. Final rotational state distributions for (a) $H_2(v = 0, j = 0)$/Cu(111) → $H_2(v' = 0, j')$/Cu(111) and (b) $H_2(v = 0, j = 0)$/Cu(111) → $H_2(v' = 1, j')$/Cu(111) as a function of j' at collision energy 1.08 eV on the RS and on the Hartree potential constructed with the VASP-SRP48 calculated normal mode frequencies at 1 K, 120 K, 300 K, 600 K, and 925 K surface temperatures.

close in agreement with experimental results (reported by Rettner *et al.*[33]) at those (higher) collision energies [see Fig. 10(b)]. The substantial broadening effects at high incidence energies as observed in these 6D QD calculations could be originating from the inclusion of vibrational degrees of freedom as obtained with SRP48 for a cluster model, adequately good accountability of the molecule–surface interaction with the SCM potential, and incorporation of the BE probability factor for the initial state distribution of vibrational modes involved in the configuration space. On the contrary, in the future, the discrimination between numerical issues and quantum effect at low collision energies could be explored systematically.

The discrepancies between the present theoretical results and experimental observations could perhaps be reduced with the inclusion of more surface modes in the effective Hartree potential to account for the bulk properties in a realistic way. Moreover, since the present effective Hartree potential considers only the linear coupling terms, inclusion of second order molecular DOF–surface mode correlation could improve the effect of broadening on the reaction probability profile. Regarding the accuracy of the SCM potential, even though QC calculation[30] using the SCM potential reproduces the AIMD sticking probabilities quite accurately, the employed normal mode configuration space with a particular frequency set, displacement vectors, and density of states (DOS) may also have been sampled beyond the acceptable region of the fitted SCM potential in this present QD calculation. On the other hand, the incompleteness of the mean-field approach to encompass the correlations between the molecular DOFs and surface modes at higher surface temperatures could be responsible for such disagreement between theory and experiment. Again, as the mean-field approach discussed here is based on a harmonic description of the surface modes, thermal lattice expansion effects are expected not to be described well.

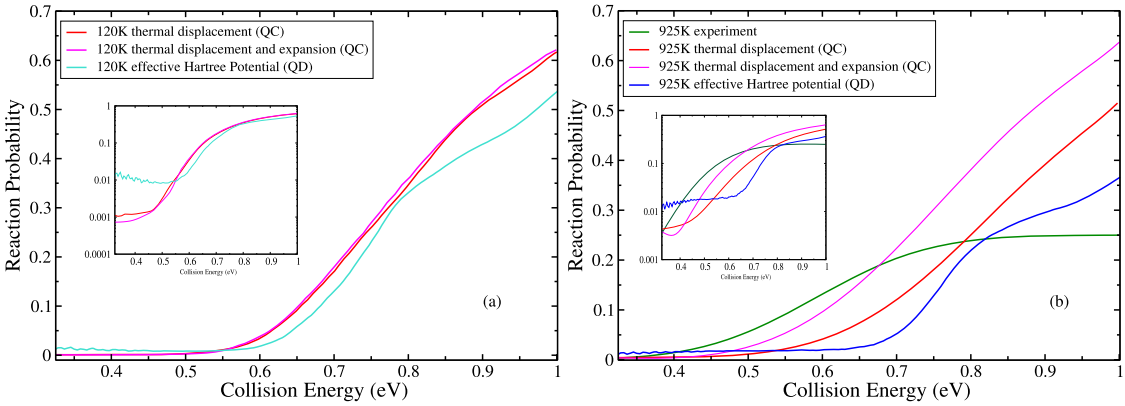

FIG. 10. Comparisons of the present QD profiles with (a) the various theoretical outcomes of the reaction probability at 120 K and (b) experimental[33] (green color) and the other theoretical results of the reaction probability at 925 K surface temperature for the H_2 ($v = 0, j = 0$)–Cu(111) system. The reaction probability profile in red color represents the QC results obtained by including the effect of thermal displacement[30] of surface atoms, whereas the magenta one depicts the effect of both thermal displacements and expansion of the metal surface[30] on the reaction probability. The turquoise and blue curves correspond to the present QD results employing the effective Hartree potential within the mean-field approximation for 120 K and 925 K surface temperatures, respectively. The reaction probabilities are also displayed in the log scale as insets. The experimental data have been extracted from Ref. 33 and are provided in Table 2 of the supplementary material.

V. CONCLUSION

In this article, we presented a formalism to take into account the role of surface vibrational modes in the reactive scattering of H_2 initially in its rovibrational ground state from the Cu(111) surface by considering a chemically accurate SCM potential within the mean-field approximation, where molecular DOFs are assumed to be only weakly coupled to the otherwise unaffected surface modes. A time and temperature dependent effective Hamiltonian has been constructed for a linearly perturbed many oscillator model, and its initial state distribution is introduced through BE and MB probability factors to incorporate the effect of surface temperature. The VASP-SRP48, FBD, and EDIM surface atom interaction potentials are used to calculate the characteristic surface frequency spectrum and the displacement vectors. The reaction and state-resolved scattering probabilities of H_2 on Cu(111) initially in the rovibrational ground state are obtained by carrying out a 6D scattering calculation with the SPO-DVR code. It appears that the distribution of initial states of normal modes with the BE probability factor and the quantization of the surface modes are the dominating factors for the broadening of reaction probabilities. Although we find substantial amount of broadening of reaction probability profiles with the increase in surface temperature, the effect is still not close enough compared to other theoretical results and experimental observations. Such deviations could arise from five limitations: (a) The mean-field approach may not be theoretically accurate enough to account for all (quantum mechanical) correlations between the molecular DOFs and surface modes. (b) Although included in the original SCM potential, the QD Hamiltonian used in this work does not account for changes in the H_2–Cu(111) interaction potential due to the thermal expansion of the surface lattice as, at this moment, it only includes the H–Cu coupling potential of the original SCM. (c) At the same time, the sampled configuration space of normal modes incorporated may be extrapolated beyond the chemically accurate fitted domain of the SCM potential. (d) The number of surface modes involved in the effective Hartree potential may not be sufficiently converged to encapsulate the actual bulk properties of the metal surface at the particular temperature. (e) Moreover, the surface mode–molecular DOF coupling scheme for constructing the effective Hartree potential could be taken into account more accurately by incorporating higher order coupling terms. (a)–(c) are particularly relevant at higher surface temperatures.

SUPPLEMENTARY MATERIAL

See the supplementary material for a brief discussion on fitting of the experimental reaction probability curve, parameters for the 6D QD calculation carried out by the SPO-DVR code, detailed descriptions of VASP-SRP48/FBD frequency and displacement vector calculation along with their relevant parameters, and comparisons among experimental and various theoretical results (presented in a tabular form).

AUTHORS' CONTRIBUTIONS

J.D. and S.M. contributed equally to this work.

ACKNOWLEDGMENTS

J.D. and S.M. acknowledge IACS for the research fellowship. J.D. and S.M. also acknowledge Mr. Soumya Mukherjee for his help in preparing this manuscript in various ways. S.A. acknowledges DST-SERB, India, for research funding under Project No. CRG/2019/000793 and thanks IACS and Leiden University for access to the super-computing facility. J.M. acknowledges the financial support from the Netherlands Organisation for Scientific Research (NWO) under VIDI Grant No. 723.014.009.

APPENDIX A: FORMULATION OF EFFECTIVE HARTREE POTENTIAL INCORPORATING LINEAR COUPLING AMONG MOLECULAR DOFs AND SURFACE MODES

The evolution operator for the surface modes under linear perturbation due to the molecule–surface interaction is defined as $U(t, t_0)$. The wavefunction for those surface modes at a time t can be obtained from the initial wavefunction at time t_0,

$$\Psi(t) = U(t, t_0)\Psi(t_0). \tag{A1}$$

The Hartree potential that arises from the initial state $\{n_0\}$ of the surface modes is defined as

$$\begin{aligned}
\langle V\rangle_{\{n_0\}} &= \langle\Psi(t)|V_I|\Psi(t)\rangle \\
&= \langle\Psi(t_0)|U^\dagger V_I U|\Psi(t_0)\rangle \\
&= \langle\{n_0\}|U^\dagger V_I U|\{n_0\}\rangle \\
&= \sum_{\{n\}}\langle\{n_0\}|U^\dagger V_I|\{n\}\rangle\langle\{n\}|U|\{n_0\}\rangle \\
&= \sum_{\{n'\}}\sum_{\{n\}}\langle\{n_0\}|U^\dagger|\{n'\}\rangle\langle\{n'\}|V_I|\{n\}\rangle\langle\{n\}|U|\{n_0\}\rangle \\
&= \sum_{\{n'\}}\sum_{\{n\}}\alpha^*_{\{n'\}\leftarrow\{n_0\}}(t)\alpha_{\{n\}\leftarrow\{n_0\}}(t)\langle\{n'\}|V_I|\{n\}\rangle.
\end{aligned} \tag{A2}$$

The amplitudes $\alpha_{\{n\}}(t)$ arise from the given initial state $\{n_0\}$ as

$$\alpha_{\{n\}\leftarrow\{n_0\}}(t) = \langle\{n\}|U|\{n_0\}\rangle. \tag{A3}$$

As the Hartree potential is implicitly dependent upon the initial state $\{n_0\}$, the formulation of such a potential certainly demands an inclusion of the distribution of states rather than a specific initial state. Therefore, the effective Hartree potential is defined as

$$\langle V\rangle(t, T_s) = \sum_{\{n_0\}} p_{\{n_0\}}\langle V\rangle_{\{n_0\}}. \tag{A4}$$

The distribution ($p_{\{n_0\}}$) should be of the BE or the MB type,

$$p_{\{n_0\}} = \prod_{k=1}^{M} p^{(k)}_{n^0_k}. \tag{A5}$$

For the quantum state (n_k^0) of normal mode (ω_k), the BE probability factor $p_{n_k^0}^{(k)}$ is defined as

$$\begin{aligned} p_{n_k^0}^{(k)} &\propto \frac{1}{\exp\left[\hbar\omega_k\left(n_k^0+\frac{1}{2}\right)\beta\right]-1} \\ &\propto z_k^{n_k^0}\cdot z_k^{1/2}\cdot\left(1-z_k^{n_k^0}\cdot z_k^{1/2}\right)^{-1} \\ &\propto z_k^{n_k^0}\cdot z_k^{1/2}+z_k^{2n_k^0}\cdot z_k+z_k^{3n_k^0}\cdot z_k^{3/2}+\cdots \\ &\propto \sum_{q=1}^{\infty}\left(z_k^{n_k^0}\right)^q (z_k)^{\frac{q}{2}}, \end{aligned} \tag{A6}$$

and the MB probability factor $p_{n_k^0}^{(k)}$ can be written as

$$\begin{aligned} p_{n_k^0}^{(k)} &\propto \exp\left[-\hbar\omega_k\left(n_k^0+\frac{1}{2}\right)\beta\right] \\ &\propto z_k^{n_k^0}\cdot z_k^{\frac{1}{2}}, \end{aligned} \tag{A7}$$

where $\beta = \frac{1}{k_b T_s}$ and $z_k = \exp\left(-\frac{\hbar\omega_k}{k_b T_s}\right)$. Diagonalization of the force constant (Hessian) matrix calculated from the surface atom interaction potential (VASP-SRP48, FBD, and EDIM) provides the frequency set ($\{\omega_k\}$) of surface modes (see Fig. 1).

The normalized probability factor for the BE or MB case is defined as

$$\tilde{p}_{n_k^0}^{(k)} = \frac{p_{n_k^0}^{(k)}}{N_{\mathrm{BE/MB}}}, \qquad \sum_k \sum_{n_k^0=0}^{\infty} \tilde{p}_{n_k^0}^{(k)} = 1, \tag{A8}$$

where

$$\begin{aligned} N_{\mathrm{BE}} &= \sum_k \sum_{n_k^0=0}^{\infty} \frac{1}{\exp\left[\hbar\omega_k\left(n_k^0+\frac{1}{2}\right)\beta\right]-1} \\ &= \sum_k \sum_{n_k^0=0}^{\infty} \sum_{q=1}^{\infty}\left(z_k^{n_k^0}\right)^q (z_k)^{\frac{q}{2}} \end{aligned} \tag{A9}$$

and

$$N_{\mathrm{MB}} = \sum_k \sum_{n_k^0=0}^{\infty} \exp\left[-\hbar\omega_k\left(n_k^0+\frac{1}{2}\right)\beta\right] = \sum_k \sum_{n_k^0=0}^{\infty} z_k^{n_k^0}\cdot z_k^{\frac{1}{2}}. \tag{A10}$$

In order to incorporate the effect of the surface mode coupling, the interaction potential (V_I) among the gas molecular DOFs and surface modes can be expanded in terms of the normal mode coordinates (Q_k's),

$$V_I = V_0 + \sum_k \lambda_k V_{k,1}\, Q_k + \frac{1}{2}\sum_{kl} \gamma_{kl} V_{kl,2}\, Q_k Q_l + \cdots, \tag{A11}$$

where V_0 is the interaction potential with the lattice atoms at the equilibrium geometry. The first ($V_{k,1}$) and second ($V_{kl,2}$) derivatives are the cause of surface mode excitations due to diatom–surface collision, and those excitations finally affect the molecular DOFs. The normal modes (Q_k's) are expressed in terms of boson creation ($b_k^\dagger$)/annihilation (b_k) operators such as $Q_k = A_k(b_k^\dagger + b_k)$ and $A_k = \sqrt{\hbar/2\omega_k}$. The signs of the first and second derivatives of the interaction potential have been taken into account by introducing λ_k and γ_{kl} as switching parameters while deriving the expression of the evolution operator perturbatively.

Considering only the linear terms, the second quantized version of the interaction potential in Eq. (A11) turns into the following form:

$$V_I = V_0 + \sum_{k=1}^{M} \lambda_k A_k (b_k F_k^- + b_k^+ F_k^+) V_{k,1}, \tag{A12}$$

where $F_k^- = \exp(-i\omega_k t)$, $F_k^+ = (F_k^-)^*$ are the modulatory terms associated with the boson ($b_k^\dagger$)/annihilation (b_k) operators in the interaction picture and $V_{k,1} = \partial V_I/\partial Q_k|_{eq}$.

For the BE or MB cases, inserting Eq. (A12) in Eq. (A2), and then in Eq. (A4), the effective Hartree potential becomes

$$\begin{aligned} \langle V\rangle(t,T_s) &= \sum_k \lambda_k \sum_{n_k^0}\sum_{n_k} \tilde{p}_{n_k^0} A_k\, V_{k,1}\Big[n_k^{1/2}\alpha^{*(k)}_{n_{k-1}\leftarrow n_k^0}(t)F_k^- \\ &\quad + (n_k+1)^{1/2}F_k^+\alpha^{*(k)}_{n_{k+1}\leftarrow n_k^0}(t)\Big]\alpha^{(k)}_{n_k\leftarrow n_k^0}(t) \\ &= \frac{1}{N_{\mathrm{BE/MB}}}\sum_k \lambda_k \sum_{n_k^0}\sum_{n_k} p_{n_k^0} A_k\, V_{k,1} \\ &\quad \times\Big[n_k^{1/2}\alpha^{*(k)}_{n_{k-1}\leftarrow n_k^0}(t)F_k^- + (n_k+1)^{1/2}F_k^+ \\ &\quad \times \alpha^{*(k)}_{n_{k+1}\leftarrow n_k^0}(t)\Big]\alpha^{(k)}_{n_k\leftarrow n_k^0}(t). \end{aligned} \tag{A13}$$

While deriving Eq. (A13), we used

$$\alpha_{\{n\}}(t) = \prod_{k=1}^{M}\alpha_{n_k}^{(k)}(t), \text{ and } \sum_{n_k}|\alpha_{n_k}^{(k)}(t)|^2 = 1, \tag{A14}$$

where $\alpha_{n_k}^{(k)}(t)$ is the amplitude for the n_kth quantum state of the mode, k is obtained from the exact solution of the linearly forced harmonic oscillator (LFHO),[75]

$$\begin{aligned} \alpha^{*(k)}_{n_k+1}(t) &= \exp\left(-i\beta_k - \frac{1}{2}\rho_k\right)[(n_k+1)!n_k^0!]^{1/2} \\ &\quad \times(-i\alpha_k^-)^{n_k-n_k^0+1} f(\rho_k, n_k+1), \end{aligned} \tag{A15}$$

and

$$\alpha_{n_k}^{(k)}(t) = \exp\left(i\beta_k - \frac{1}{2}\rho_k\right)[n_k!n_k^0!]^{1/2}(i\alpha_k^+)^{n_k-n_k^0} f(\rho_k, n_k). \tag{A16}$$

The terms ρ_k, $\alpha_k^\pm$, and β_k of Eqs. (A15) and (A16) are expressed as

$$\rho_k = \alpha_k^+\alpha_k^-, \tag{A17}$$

$$\alpha_k^\pm = -\frac{A_k}{\hbar}\int_{t_0}^{t} dt' V_{k,1}\exp[\pm i\omega_k t'], \tag{A18}$$

and

$$\beta_k = \frac{i}{\hbar}\int_{t_0}^{t} dt' V_{k,1}\{\exp[i\omega_k t']\alpha_k^-(t') - \exp[-i\omega_k t']\alpha_k^+(t')\}. \quad \text{(A19)}$$

$f(\rho_k, n_k)$ is written as

$$f(\rho_k, n_k) = \frac{1}{n_k!} L_{n_k^0}^{n_k - n_k^0}(\rho_k), \quad n_k \geq n_k^0, \quad \text{(A20)}$$

and

$$f(\rho_k, n_k) = \frac{1}{n_k^0!}(-\rho_k)^{n_k^0 - n_k} L_{n_k}^{n_k^0 - n_k}(\rho_k), \quad n_k < n_k^0, \quad \text{(A21)}$$

where $L_{n_k}^{n_k^0 - n_k}$ is the Laguerre-polynomial.

Inserting Eqs. (A15)–(A21) in Eq. (A13) and employing the BE or the MB factor for the initial distribution, we obtain

$$\langle V\rangle(t, T_s) = \frac{1}{N_{\text{BE/MB}}}\sum_k \left(S_I^{(k)}(t, T_s) + S_{II}^{(k)}(t, T_s)\right), \quad \text{(A22)}$$

where

$$S_I^{(k)}(t, T_s) = -\omega_k^{-1}\epsilon_k(t)\exp(-\rho_k)\sum_{q=1}^{\infty}(z_k)^{q/2}\sum_{n_k^0=1}^{\infty}\sum_{m=0}^{n_k^0-1}\left(z_k^q\right)^{n_k^0} \times \frac{m!}{n_k^0!}(\rho_k)^{n_k^0-m} L_m^{n_k^0-m}(\rho_k) \times L_{m-1}^{n_k^0-m+1}(\rho_k) \quad \text{for the BE case} \quad \text{(A23)}$$

and

$$S_I^{(k)}(t, T_s) = -\omega_k^{-1}\epsilon_k(t)\exp(-\rho_k) z_k^{1/2}\sum_{n_k^0=1}^{\infty}\sum_{m=0}^{n_k^0-1} z_k^{n_k^0}\frac{m!}{n_k^0!} \times (\rho_k)^{n_k^0-m} L_m^{n_k^0-m}(\rho_k) \times L_{m-1}^{n_k^0-m+1}(\rho_k) \quad \text{for the MB case.} \quad \text{(A24)}$$

The expression of $S_I^{(k)}(t, T_s)$ can be rearranged as

$$S_I^{(k)}(t, T_s) = -\omega_k^{-1}\epsilon_k(t)\exp(-\rho_k)\sum_{q=1}^{\infty}(z_k)^{q/2}\sum_{n=0}^{\infty}\sum_{m=0}^{\infty}\left(z_k^q\right)^{m+n} \times \frac{n!}{(n+m)!}(\rho_k)^m L_n^m \times (\rho_k) L_{n-1}^{m+1}(\rho_k) \quad \text{for the BE case} \quad \text{(A25)}$$

and

$$S_I^{(k)}(t, T_s) = -\omega_k^{-1}\epsilon_k(t)\exp(-\rho_k) z_k^{1/2}\sum_{n=0}^{\infty}\sum_{m=0}^{\infty} z_k^{m+n}\frac{n!}{(n+m)!} \times (\rho_k)^m L_n^m(\rho_k) \times L_{n-1}^{m+1}(\rho_k) \quad \text{for the MB case.} \quad \text{(A26)}$$

Similarly, the second term $S_{II}^{(k)}(t, T_s)$ in Eq. (A22) can be expressed as

$$S_{II}^{(k)}(t, T_s) = \omega_k^{-1}\epsilon_k(t)\exp(-\rho_k)\sum_{q=1}^{\infty}(z_k)^{q/2}\sum_{n_k^0=0}^{\infty}\sum_{m=n_k^0}^{\infty}\left(z_k^q\right)^{n_k^0} \times \frac{n_k^0!}{m!}(\rho_k)^{m-n_k^0} L_m^{m-n_k^0}(\rho_k) \times L_m^{m-n_k^0+1}(\rho_k) \quad \text{for the BE case} \quad \text{(A27)}$$

and

$$S_{II}^{(k)}(t, T_s) = \omega_k^{-1}\epsilon_k(t)\exp(-\rho_k) z_k^{1/2}\sum_{n_k^0=0}^{\infty}\sum_{m=n_k^0}^{\infty} z_k^{n_k^0}\frac{n_k^0!}{m!} \times (\rho_k)^{m-n_k^0} L_m^{m-n_k^0}(\rho_k) \times L_m^{m-n_k^0+1}(\rho_k) \quad \text{for the MB case,} \quad \text{(A28)}$$

which may be rewritten as

$$S_{II}^{(k)}(t, T_s) = \omega_k^{-1}\epsilon_k(t)\exp(-\rho_k)\sum_{q=1}^{\infty}(z_k)^{q/2}\sum_{n=0}^{\infty}\sum_{m=0}^{\infty}\left(z_k^q\right)^{n} \times \frac{n!}{(n+m)!}(\rho_k)^m L_n^m(\rho_k) \times L_n^{m+1}(\rho_k) \quad \text{for the BE case} \quad \text{(A29)}$$

and

$$S_{II}^{(k)}(t, T_s) = \omega_k^{-1}\epsilon_k(t)\exp(-\rho_k)\sum_{q=1}^{\infty} z_k^{1/2}\sum_{n=0}^{\infty}\sum_{m=0}^{\infty} z_k^{n}\frac{n!}{(n+m)!} \times (\rho_k)^m L_n^m(\rho_k) L_n^{m+1}(\rho_k) \quad \text{for the MB case.} \quad \text{(A30)}$$

In Eqs. (A25)–(A30), the explicit time dependent quantity $\epsilon_k(t)$ is defined as

$$\epsilon_k(t) = \lambda_k V_{k,1}\int_{t_0}^{t} dt' V_{k,1}\sin\left[\omega_k\left(t' - t\right)\right]. \quad \text{(A31)}$$

Since the first derivative of the interaction potential ($V_{k,1}$) is time independent, it can be taken out of the integral and the integration over time can be performed analytically.

Applying Eqs. (A25) and (A29) in Eq. (A22), the form of the effective potential has been turned into the following form for the BE case:

$$\langle V\rangle(t,T_s)=\frac{1}{N_{BE}}\sum_k\omega_k^{-1}\epsilon_k(t)\exp(-\rho_k)\Bigg\{\sum_{q=1}^{\infty}(z_k)^{q/2}\sum_{n=0}^{\infty}\sum_{m=0}^{\infty}\left(z_k^q\right)^{n+m}\frac{n!}{(n+m)!}(\rho_k)^m L_n^m(\rho_k)L_n^m(\rho_k)$$
$$+\sum_{q=1}^{\infty}(z_k)^{q/2}\sum_{n=0}^{\infty}\sum_{m=0}^{\infty}\left(z_k^q\right)^{n}\frac{n!}{(n+m)!}(\rho_k)^m L_n^m(\rho_k)L_n^m(\rho_k)+\sum_{q=1}^{\infty}(z_k)^{q/2}\sum_{n=0}^{\infty}\sum_{m=0}^{\infty}\left(z_k^q\right)^{n}$$
$$\times\frac{n!}{(n+m)!}(\rho_k)^m L_n^m(\rho_k)L_{n-1}^m(\rho_k)-\sum_{q=1}^{\infty}(z_k)^{q/2}\sum_{n=0}^{\infty}\sum_{m=0}^{\infty}\left(z_k^q\right)^{n+m}\frac{n!}{(n+m)!}(\rho_k)^m L_n^m(\rho_k)L_n^{m+1}(\rho_k)\Bigg\}. \tag{A32}$$

Similarly, the expression of the effective potential for the MB factor is

$$\langle V\rangle(t,T_s)=\frac{1}{N_{MB}}\sum_k\omega_k^{-1}\epsilon_k(t)\exp(-\rho_k)$$
$$\times\Bigg\{z_k^{1/2}\sum_{n=0}^{\infty}\sum_{m=0}^{\infty}z_k^{n+m}\frac{n!}{(n+m)!}(\rho_k)^m L_n^m(\rho_k)$$
$$\times L_n^m(\rho_k)+z_k^{1/2}\sum_{n=0}^{\infty}\sum_{m=0}^{\infty}z_k^{n}\frac{n!}{(n+m)!}(\rho_k)^m$$
$$\times L_n^m(\rho_k)L_n^m(\rho_k)+z_k^{1/2}\sum_{n=0}^{\infty}\sum_{m=0}^{\infty}z_k^{n}\frac{n!}{(n+m)!}(\rho_k)^m$$
$$\times L_n^m(\rho_k)L_{n-1}^m(\rho_k)-z_k^{1/2}\sum_{n=0}^{\infty}\sum_{m=0}^{\infty}z_k^{n+m}\frac{n!}{(n+m)!}$$
$$\times(\rho_k)^m L_n^m(\rho_k)L_n^{m+1}(\rho_k)\Bigg\}. \tag{A33}$$

The following identity:

$$\sum_{p=0}^{\infty}p!\,L_p^{\alpha}(x)L_p^{\alpha}(y)\frac{z^p}{(p+\alpha)!}=\left[\frac{(xyz)^{-\frac{\alpha}{2}}}{(1-z)}\right]\exp\left[-\frac{z(x+y)}{(1-z)}\right]$$
$$\times I_{\alpha}\left[2(xyz)^{\frac{1}{2}}/(1-z)\right],$$

has been plugged in Eqs. (A32) and (A33) to arrive at a more simplified form for both the BE and MB cases, respectively,

$$\langle V\rangle(t,T_s)=\frac{1}{N_{BE}}\sum_k\omega_k^{-1}\epsilon_k(t)\sum_{q=1}^{\infty}\frac{z_k^{q/2}}{(1-z_k^q)}$$
$$\times\exp\left[\rho_k(1+z_k^q)/(z_k^q-1)\right]$$
$$\times\{S_k^{q+}(t,T_s)+S_k^{q-}(t,T_s)-I_0(t_k^q)\}\quad\text{for the BE case} \tag{A34}$$

and

$$\langle V\rangle(t,T_s)=\frac{1}{N_{MB}}\sum_k\omega_k^{-1}\epsilon_k(t)\frac{z_k^{1/2}}{(1-z_k)}\exp\left[\rho_k(1+z_k)/(z_k-1)\right]$$
$$\times\{S_k^{+}(t,T_s)+S_k^{-}(t,T_s)-I_0(t_k)\}\quad\text{for the MB case,} \tag{A35}$$

where the terms $S_k^{q\pm}(t,T_s)$ can be expressed as $S_k^{q\pm}(t,T_s)=\sum_{m=0}^{\infty}(z_k^q)^{\pm m/2}I_m(t_k^q)$ by using the modified Bessel-function of the first kind $I_m(t_k^q)$ and $t_k^q=2\rho_k(z_k^q)^{1/2}/(1-z_k^q)$.

As $S_k^{q+}(t,T_s)+S_k^{q-}(t,T_s)-I_0(t_k^q)=\exp[\rho_k(1+z_k^q)/(1-z_k^q)]$ ($q=1,2,3,\ldots$), the expression in Eqs. (A34) and (A35) is further simplified to

$$\langle V\rangle(t,T_s)=\frac{1}{N_{BE}}\sum_k\omega_k^{-1}\epsilon_k(t)\sum_{q=1}^{\infty}\frac{z_k^{q/2}}{(1-z_k^q)}\qquad\text{for the BE case} \tag{A36}$$

and

$$\langle V\rangle(t,T_s)=\frac{1}{N_{MB}}\sum_k\omega_k^{-1}\epsilon_k(t)\frac{z_k^{1/2}}{(1-z_k)}\qquad\text{for the MB case.} \tag{A37}$$

Thus, the final form of the effective Hartree potential for the BE case is written as

$$V_{\text{eff}}^{BE}(R,\theta,\phi,X,Y,Z,t,T_s)$$
$$=\frac{1}{N_{BE}}\sum_{k=7}^{3N}\lambda_k\frac{1}{\omega_k^2}V_{k,1}^2[\cos\omega_k(t-t_0)-1]\sum_{q=1}^{\infty}\frac{z_k^{q/2}}{(1-z_k^q)}, \tag{A38}$$

and for the MB case,

$$V_{\text{eff}}^{MB}(R,\theta,\phi,X,Y,Z,t,T_s)$$
$$=\frac{1}{N_{MB}}\sum_{k=7}^{3N}\lambda_k\frac{1}{\omega_k^2}V_{k,1}^2[\cos\omega_k(t-t_0)-1]\frac{z_k^{1/2}}{(1-z_k)}. \tag{A39}$$

The normalization for the BE or MB cases can be simplified as

$$N_{BE}=\sum_k\sum_{n_k^0=0}^{\infty}\sum_{q=1}^{\infty}\left(z_k^{n_k^0}\right)^q(z_k)^{\frac{q}{2}}$$
$$=\sum_k\sum_{q=1}^{\infty}(z_k)^{\frac{q}{2}}\sum_{n_k^0=0}^{\infty}\exp\left[-\frac{qn_k^0\hbar\omega_k}{k_bT_s}\right]=\sum_k\sum_{q=1}^{\infty}\frac{(z_k)^{\frac{q}{2}}}{(1-z_k^q)} \tag{A40}$$

and

$$N_{MB}=\sum_k\sum_{n_k^0=0}^{\infty}z_k^{n_k^0}\cdot z_k^{\frac{1}{2}}=\sum_k z_k^{\frac{1}{2}}\sum_{n_k^0=0}^{\infty}\exp\left[-\frac{n_k^0\hbar\omega_k}{k_bT_s}\right]$$
$$=\sum_k\frac{z_k^{\frac{1}{2}}}{(1-z_k)}. \tag{A41}$$

APPENDIX B: EVOLUTION OF FIRST DERIVATIVE OF THE INTERACTION POTENTIAL WITH RESPECT TO METAL ATOM POSITION $\left(\frac{\partial V_{a\alpha}^{\text{Cu-H}}}{\partial X_{\alpha i}}\right)$

The interaction potential between a metal (Cu) atom of the surface and a gas atom of the molecule is written as[30]

$$V_{a\alpha}^{\text{Cu-H}}(r_{a\alpha}) = (1-\rho(r_{a\alpha}))V_{\text{Ryd}}(r_{a\alpha}) + \rho(r_{a\alpha})V_{\text{Ryd}}(b_2), \tag{B1}$$

where $V_{\text{Ryd}}(r_{a\alpha})$ can be defined as

$$V_{\text{Ryd}}(r_{a\alpha}) = -\exp\{-l(r_{a\alpha}-z)\}\sum_{k=0}^{3}(c_k(r_{a\alpha}-z)^k) \tag{B2}$$

and $\rho(r_{a\alpha})$ is expressed as

$$\rho(r_{a\alpha}) = \begin{cases} 0 & \text{if } r_{a\alpha} < b_2, \\ \frac{1}{2}\cos\left(\frac{\pi(r_{a\alpha}-b_2)}{b_2-b_1}\right)+\frac{1}{2} & \text{if } b_1 \le r_{a\alpha} \le b_2, \\ 1 & \text{if } r_{a\alpha} > b_2. \end{cases} \tag{B3}$$

The interaction potential $[V_{a\alpha}^{\text{Cu-H}}(r_{a\alpha})]$ as displayed in Eqs. (B1)–(B3) is a function of the gas–metal distance ($r_{a\alpha}$) with Rydberg parameters (b_1, b_2, c_0, c_1, c_2, c_3, l, z). Those parameters (P_i) are dependent on the two quantities $P_{i,\text{I}}$ and $P_{i,\text{II}}$, which are related to the H–H separation (R) and a pure two-body, H–Cu ($r_{a\alpha}$) component of three-body SCM potential, respectively,

$$P_i = \begin{cases} P_{i,\text{I}}R_{\min} + P_{i,\text{II}} & \text{if } R < R_{\min}, \\ P_{i,\text{I}}R + P_{i,\text{II}} & \text{if } R_{\min} \le R \le R_{\max}, \\ P_{i,\text{I}}R_{\max} + P_{i,\text{II}} & \text{if } R > R_{\max}. \end{cases} \tag{B4}$$

The first derivative of the interaction potential is given by

$$\left[\frac{\partial V_{a\alpha}^{\text{Cu-H}}(r_{a\alpha}^{\text{id}})}{\partial X_{\alpha i}}\right] = 0 \tag{B5}$$

and

$$\frac{\partial V_{a\alpha}^{\text{Cu-H}}(r_{a\alpha})}{\partial X_{\alpha i}} = \begin{cases} \left[-lV_{\text{Ryd}}(r_{a\alpha}) - \exp\{-l(r_{a\alpha}-z)\}\right. \\ \left.\times\left(c_1+2c_2(r_{a\alpha}-z)+3c_3(r_{a\alpha}-z)^2\right)\right]\left(\frac{X_{ai}-X_{ai}}{r_{a\alpha}}\right) & \text{if } r_{a\alpha} < b_2, \\ \left[\frac{1}{2}\sin\left(\frac{\pi(r_{a\alpha}-b_2)}{b_2-b_1}\right)\left(\frac{\pi}{b_2-b_1}\right)\left(V_{\text{Ryd}}(r_{a\alpha}) - V_{\text{Ryd}}(b_2)\right)\right. \\ +(1-\rho(r_{a\alpha}))\{-lV_{\text{Ryd}}(r_{a\alpha}) - \exp\{-l(r_{a\alpha}-z)\}\} \\ \left.\times\left(c_1+2c_2(r_{a\alpha}-z)+3c_3(r_{a\alpha}-z)^2\right)\}\right]\left(\frac{X_{ai}-X_{ai}}{r_{a\alpha}}\right) & \text{if } b_1 \le r_{a\alpha} \le b_2, \\ 0 & \text{if } r_{a\alpha} > b_2. \end{cases} \tag{B6}$$

1. Evolution of $\left[\frac{\partial V_{a\alpha}^{\text{Cu-H}}(r_{a\alpha}^{\text{id}})}{\partial X_{\alpha i}}\right]$

$$r_{a\alpha}^{\text{id}} = \sqrt{\sum_i (X_{ai} - X_{\alpha i}^{\text{id}})^2}, \qquad \frac{\partial r_{a\alpha}^{\text{id}}}{\partial X_{\alpha i}} = 0, \tag{B7}$$

$$\therefore \left[\frac{\partial V_{a\alpha}^{\text{Cu-H}}(r_{a\alpha}^{\text{id}})}{\partial X_{\alpha i}}\right] = \frac{\partial V_{a\alpha}^{\text{Cu-H}}(r_{a\alpha}^{\text{id}})}{\partial r_{a\alpha}^{\text{id}}}\cdot\frac{\partial r_{a\alpha}^{\text{id}}}{\partial X_{\alpha i}} = 0. \tag{B8}$$

2. Evolution of $\left[\frac{\partial V_{a\alpha}^{\text{Cu-H}}(r_{a\alpha})}{\partial X_{\alpha i}} = \frac{\partial V_{a\alpha}^{\text{Cu-H}}(r_{a\alpha})}{\partial r_{a\alpha}}\cdot\frac{\partial r_{a\alpha}}{\partial X_{\alpha i}}\right]$

$$\frac{\partial r_{a\alpha}}{\partial X_{\alpha i}} = \frac{X_{\alpha i} - X_{ai}}{r_{a\alpha}}, \tag{B9}$$

$$\begin{aligned} \frac{\partial V_{a\alpha}^{\text{Cu-H}}(r_{a\alpha})}{\partial r_{a\alpha}} &= \frac{\partial}{\partial r_{a\alpha}}\left[(1-\rho(r_{a\alpha}))V_{\text{Ryd}}(r_{a\alpha}) + \rho(r_{a\alpha})V_{\text{Ryd}}(b_2)\right] \\ &= -\frac{\partial\rho(r_{a\alpha})}{\partial r_{a\alpha}}V_{\text{Ryd}}(r_{a\alpha}) + (1-\rho(r_{a\alpha}))\frac{\partial V_{\text{Ryd}}(r_{a\alpha})}{\partial r_{a\alpha}} + \frac{\partial\rho(r_{a\alpha})}{\partial r_{a\alpha}}V_{\text{Ryd}}(b_2) + \rho(r_{a\alpha})\frac{\partial V_{\text{Ryd}}(b_2)}{\partial r_{a\alpha}}, \end{aligned} \tag{B10}$$

where $r_{a\alpha} = \sqrt{\sum_i (X_{ai} - X_{\alpha i})^2}$ and $\rho(r_{a\alpha})\frac{\partial V_{\mathrm{Ryd}}(b_2)}{\partial r_{a\alpha}} = 0$ as $V_{\mathrm{Ryd}}(b_2)$ is independent of $r_{a\alpha}$.

a. If $r_{a\alpha} < b_2$

In this range, $\rho(r_{a\alpha}) = 0$ and $\frac{\partial \rho(r_{a\alpha})}{\partial r_{a\alpha}} = 0$.

$$\frac{\partial V_{a\alpha}^{\text{Cu-H}}(r_{a\alpha})}{\partial r_{a\alpha}} = \frac{\partial V_{\mathrm{Ryd}}(r_{a\alpha})}{\partial r_{a\alpha}} = \frac{\partial}{\partial r_{a\alpha}}\left[-\exp\{-l(r_{a\alpha}-z)\}\sum_{k=0}^{3}(c_k(r_{a\alpha}-z)^k)\right]$$
$$= -lV_{\mathrm{Ryd}}(r_{a\alpha}) - \exp\{-l(r_{a\alpha}-z)\}\left[c_1 + 2c_2(r_{a\alpha}-z) + 3c_3(r_{a\alpha}-z)^2\right], \tag{B11}$$

$$\therefore \frac{\partial V_{a\alpha}^{\text{Cu-H}}(r_{a\alpha})}{\partial r_{a\alpha}}\cdot\frac{\partial r_{a\alpha}}{\partial X_{\alpha i}} = \left[-lV_{\mathrm{Ryd}}(r_{a\alpha}) - \exp\{-l(r_{a\alpha}-z)\}\left[c_1 + 2c_2(r_{a\alpha}-z) + 3c_3(r_{a\alpha}-z)^2\right]\right]\left(\frac{X_{\alpha i} - X_{ai}}{r_{a\alpha}}\right). \tag{B12}$$

b. If $b_1 \le r_{a\alpha} \le b_2$

In this range, $\rho(r_{a\alpha}) = \frac{1}{2}\cos\left(\frac{\pi(r_{a\alpha}-b_2)}{b_2-b_1}\right) + \frac{1}{2}$ and $\frac{\partial \rho(r_{a\alpha})}{\partial r_{a\alpha}} = -\frac{1}{2}\sin\left(\frac{\pi(r_{a\alpha}-b_2)}{b_2-b_1}\right)\frac{\pi}{b_2-b_1}$,

$$\frac{\partial V_{a\alpha}^{\text{Cu-H}}(r_{a\alpha})}{\partial r_{a\alpha}} = \frac{1}{2}\sin\left(\frac{\pi(r_{a\alpha}-b_2)}{b_2-b_1}\right)\left(\frac{\pi}{b_2-b_1}\right)V_{\mathrm{Ryd}}(r_{a\alpha}) + (1-\rho(r_{a\alpha}))\frac{\partial V_{\mathrm{Ryd}}(r_{a\alpha})}{\partial r_{a\alpha}}$$
$$-\frac{1}{2}\sin\left(\frac{\pi(r_{a\alpha}-b_2)}{b_2-b_1}\right)\left(\frac{\pi}{b_2-b_1}\right)V_{\mathrm{Ryd}}(b_2)$$
$$= \frac{1}{2}\sin\left(\frac{\pi(r_{a\alpha}-b_2)}{b_2-b_1}\right)\left(\frac{\pi}{b_2-b_1}\right)\left(V_{\mathrm{Ryd}}(r_{a\alpha}) - V_{\mathrm{Ryd}}(b_2)\right) + (1-\rho(r_{a\alpha}))$$
$$\times\left[-lV_{\mathrm{Ryd}}(r_{a\alpha}) - \exp\{-l(r_{a\alpha}-z)\}\left[c_1 + 2c_2(r_{a\alpha}-z) + 3c_3(r_{a\alpha}-z)^2\right]\right], \tag{B13}$$

where $\frac{\partial V_{\mathrm{Ryd}}(r_{a\alpha})}{\partial r_{a\alpha}} = -lV_{\mathrm{Ryd}}(r_{a\alpha}) - \exp\{-l(r_{a\alpha}-z)\}\left[c_1 + 2c_2(r_{a\alpha}-z) + 3c_3(r_{a\alpha}-z)^2\right]$.

$$\therefore\frac{\partial V_{a\alpha}^{\text{Cu-H}}(r_{a\alpha})}{\partial r_{a\alpha}}\cdot\frac{\partial r_{a\alpha}}{\partial X_{\alpha i}} = \left[\frac{1}{2}\sin\left(\frac{\pi(r_{a\alpha}-b_2)}{b_2-b_1}\right)\left(\frac{\pi}{b_2-b_1}\right)\left(V_{\mathrm{Ryd}}(r_{a\alpha}) - V_{\mathrm{Ryd}}(b_2)\right)\right.$$
$$+ (1-\rho(r_{a\alpha}))\left[-lV_{\mathrm{Ryd}}(r_{a\alpha}) - \exp\{-l(r_{a\alpha}-z)\}\right.$$
$$\left.\left.\times\left[c_1 + 2c_2(r_{a\alpha}-z) + 3c_3(r_{a\alpha}-z)^2\right]\right]\right]\left(\frac{X_{\alpha i} - X_{ai}}{r_{a\alpha}}\right). \tag{B14}$$

c. If $r_{a\alpha} > b_2$

In this range, $\rho(r_{a\alpha}) = 1$ and $\frac{\partial \rho(r_{a\alpha})}{\partial r_{a\alpha}} = 0$,

$$\frac{\partial V_{a\alpha}^{\text{Cu-H}}(r_{a\alpha})}{\partial r_{a\alpha}} = \frac{\partial V_{\mathrm{Ryd}}(b_2)}{\partial r_{a\alpha}} = 0, \tag{B15}$$

since $V_{\mathrm{Ryd}}(b_2)$ is independent of the gas–metal atom distance $r_{a\alpha}$.

$$\therefore \frac{\partial V_{a\alpha}^{\text{Cu-H}}(r_{a\alpha})}{\partial r_{a\alpha}}\cdot\frac{\partial r_{a\alpha}}{\partial X_{\alpha i}} = 0. \tag{B16}$$

DATA AVAILABILITY

The data that support the findings of this study are available within this article and its supplementary material.

REFERENCES

[1] G. Anger, A. Winkler, and K. D. Rendulic, Surf. Sci. **220**, 1 (1989).
[2] E. Watts and G. O. Sitz, J. Chem. Phys. **114**, 4171 (2001).
[3] H. A. Michelsen, C. T. Rettner, and D. J. Auerbach, Surf. Sci. **272**, 65 (1992).
[4] C. T. Rettner, H. A. Michelsen, and D. J. Auerbach, Faraday Discuss. **96**, 17 (1993).
[5] C. T. Rettner, D. J. Auerbach, and H. A. Michelsen, Phys. Rev. Lett. **68**, 1164 (1992).
[6] H. F. Berger, M. Leisch, A. Winkler, and K. D. Rendulic, Chem. Phys. Lett. **175**, 425 (1990).
[7] H. Hou, S. J. Gulding, C. T. Rettner, A. M. Wodtke, and D. J. Auerbach, Science **277**, 80 (1997).
[8] M. J. Murphy and A. Hodgson, J. Chem. Phys. **108**, 4199 (1998).
[9] R. C. Mowrey, G. J. Kroes, and E. J. Baerends, J. Chem. Phys. **108**, 6906 (1998).
[10] Z. S. Wang, G. R. Darling, and S. Holloway, Phys. Rev. Lett. **87**, 226102 (2001).
[11] S. Nave and B. Jackson, Phys. Rev. Lett. **98**, 173003 (2007).
[12] A. K. Tiwari, S. Nave, and B. Jackson, Phys. Rev. Lett. **103**, 253201 (2009).
[13] A. K. Tiwari, S. Nave, and B. Jackson, J. Chem. Phys. **132**, 134702 (2010).
[14] G. D. Billing, Phys. Chem. Chem. Phys. **4**, 2865 (2002).
[15] C. Díaz, E. Pijper, R. A. Olsen, H. F. Busnengo, D. J. Auerbach, and G. J. Kroes, Science **326**, 832 (2009).

[16]M. Bonfanti, C. Díaz, M. F. Somers, and G. J. Kroes, Phys. Chem. Chem. Phys. **13**, 4552 (2011).
[17]E. Watts, G. O. Sitz, D. A. McCormack, G. J. Kroes, R. A. Olsen, J. A. Groeneveld, J. N. P. Van Stralen, E. J. Baerends, and R. C. Mowrey, J. Chem. Phys. **114**, 495 (2001).
[18]M. Hand and J. Harris, J. Chem. Phys. **92**, 7610 (1990).
[19]A. C. Luntz and M. Persson, J. Chem. Phys. **123**, 074704-1 (2005).
[20]M. Dohle and P. Saalfrank, Surf. Sci. **373**, 95 (1997).
[21]F. Lüder, M. Nest, and P. Saalfrank, Theor. Chem. Acc. **127**, 183 (2010).
[22]J. Dai and J. C. Light, J. Chem. Phys. **108**, 7816 (1998).
[23]J. Dai and J. C. Light, J. Chem. Phys. **107**, 1676 (1997).
[24]M. F. Somers, S. M. Kingma, E. Pijper, G. J. Kroes, and D. Lemoine, Chem. Phys. Lett. **360**, 390 (2002).
[25]S. Adhikari and G. D. Billing, J. Chem. Phys. **112**, 3884 (2000).
[26]T. Sahoo, S. Sardar, and S. Adhikari, Phys. Chem. Chem. Phys. **13**, 10100 (2011).
[27]T. Sahoo, S. Sardar, P. Mondal, B. Sarkar, and S. Adhikari, J. Phys. Chem. A **115**, 5256 (2011).
[28]T. Sahoo, S. Sardar, and S. Adhikari, Phys. Scr. **84**, 028105-1 (2011).
[29]T. Sahoo, S. Mukherjee, and S. Adhikari, J. Chem. Phys. **136**, 084306-1 (2012).
[30]M. Wijzenbroek and M. F. Somers, J. Chem. Phys. **137**, 054703 (2012).
[31]P. Spiering, M. Wijzenbroek, and M. F. Somers, J. Chem. Phys. **149**, 234702 (2018).
[32]F. Nattino, A. Genova, M. Guijt, A. S. Muzas, C. Díaz, D. J. Auerbach, and G.-J. Kroes, J. Chem. Phys. **141**, 124705 (2014).
[33]C. T. Rettner, H. A. Michelsen, and D. J. Auerbach, J. Chem. Phys. **102**, 4625 (1995).
[34]C. T. Rettner, H. A. Michelsen, and D. J. Auerbach, Chem. Phys. **175**, 157 (1993).
[35]H. A. Michelsen, C. T. Rettner, D. J. Auerbach, and R. N. Zare, J. Chem. Phys. **98**, 8294 (1993).
[36]H. A. Michelsen and D. J. Auerbach, J. Chem. Phys. **94**, 7502 (1991).
[37]S. Kaufmann, Q. Shuai, D. J. Auerbach, D. Schwarzer, and A. M. Wodtke, J. Chem. Phys. **148**, 194703 (2018).
[38]G. Wiesenekker, G. J. Kroes, and E. J. Baerends, J. Chem. Phys. **104**, 7344 (1996).
[39]C. Díaz, R. A. Olsen, D. J. Auerbach, and G. J. Kroes, Phys. Chem. Chem. Phys. **12**, 6499 (2010).
[40]G.-J. Kroes, Phys. Chem. Chem. Phys. **14**, 14966 (2012).
[41]A. Mondal, M. Wijzenbroek, M. Bonfanti, C. Díaz, and G.-J. Kroes, J. Phys. Chem. A **117**, 8770 (2013).
[42]B. Jiang and H. Guo, J. Chem. Phys. **139**, 054112 (2013).
[43]B. Jiang and H. Guo, J. Chem. Phys. **141**, 034109 (2014).
[44]B. Jiang, J. Li, and H. Guo, Int. Rev. Phys. Chem. **35**, 479 (2016).
[45]J. Behler and M. Parrinello, Phys. Rev. Lett. **98**, 146401 (2007).
[46]B. Kolb, X. Luo, X. Zhou, B. Jiang, and H. Guo, J. Phys. Chem. Lett. **8**, 666 (2017).
[47]Q. Liu, X. Zhou, L. Zhou, Y. Zhang, X. Luo, H. Guo, and B. Jiang, J. Phys. Chem. C **122**, 1761 (2018).
[48]B. Jiang and H. Guo, J. Chem. Phys. **144**, 091101 (2016).
[49]Y. Zhang, X. Zhou, and B. Jiang, J. Phys. Chem. Lett. **10**, 1185 (2019).
[50]M. d. Cueto, X. Zhou, L. Zhou, Y. Zhang, B. Jiang, and H. Guo, J. Phys. Chem. C **124**, 5174 (2020).
[51]R. Yin, Y. Zhang, and B. Jiang, J. Phys. Chem. Lett. **10**, 5969 (2019).
[52]K. Shakouri, J. Behler, J. Meyer, and G.-J. Kroes, J. Phys. Chem. Lett. **8**, 2131 (2017).
[53]N. Gerrits, K. Shakouri, J. Behler, and G.-J. Kroes, J. Phys. Chem. Lett. **10**, 1763 (2019).
[54]L. Zhu, Y. Zhang, L. Zhang, X. Zhou, and B. Jiang, Phys. Chem. Chem. Phys. **22**, 13958 (2020).
[55]Y. Zhang, C. Hu, and B. Jiang, J. Phys. Chem. Lett. **10**, 4962 (2019).
[56]B. Jiang and H. Guo, Phys. Chem. Chem. Phys. **16**, 24704 (2014).
[57]B. Jiang, X. Hu, S. Lin, D. Xie, and H. Guo, Phys. Chem. Chem. Phys. **17**, 23346 (2015).
[58]T. Liu, B. Fu, and D. H. Zhang, J. Chem. Phys. **139**, 184705 (2013).
[59]T. Liu, B. Fu, and D. H. Zhang, J. Chem. Phys. **140**, 144701 (2014).
[60]T. Liu, B. Fu, and D. H. Zhang, J. Chem. Phys. **151**, 144707 (2019).
[61]H. F. Busnengo, A. Salin, and W. Dong, J. Chem. Phys. **112**, 7641 (2000).
[62]N. Pineau, H. F. Busnengo, J. C. Rayez, and A. Salin, J. Chem. Phys. **122**, 214705 (2005).
[63]R. A. Olsen, H. F. Busnengo, A. Salin, M. F. Somers, G. J. Kroes, and E. J. Baerends, J. Chem. Phys. **116**, 3841 (2002).
[64]F. Nattino, C. Díaz, B. Jackson, and G.-J. Kroes, Phys. Rev. Lett. **108**, 236104 (2012).
[65]G.-J. Kroes, J. Phys. Chem. Lett. **6**, 4106 (2015).
[66]M. Dohle, P. Saalfrank, and T. Uzer, J. Chem. Phys. **108**, 4226 (1998).
[67]M. Dohle, P. Saalfrank, and T. Uzer, Surf. Sci. **409**, 37 (1998).
[68]P. Saalfrank and W. H. Miller, Surf. Sci. **303**, 206 (1994).
[69]H. F. Busnengo, W. Dong, P. Sautet, and A. Salin, Phys. Rev. Lett. **87**, 127601 (2001).
[70]S. Nave and B. Jackson, J. Chem. Phys. **127**, 224702 (2007).
[71]S. Mandal, T. Sahoo, S. Ghosh, and S. Adhikari, Mol. Phys. **113**, 3042 (2015).
[72]S. Mandal, S. Ghosh, S. S. Sardar, and S. Adhikari, Int. Rev. Phys. Chem. **37**, 607 (2019).
[73]S. Mandal, T. Sahoo, S. Ghosh, and S. Adhikari, J. Theor. Comput. Chem. **14**, 1550028 (2015).
[74]T. N. Truong, D. G. Truhlar, and B. C. Garrett, J. Phys. Chem. **93**, 8227 (1989).
[75]P. Pechukas and J. C. Light, J. Chem. Phys. **44**, 3897 (1966).
[76]M. D. Feit, J. A. Fleck, and A. Steiger, J. Comput. Phys. **47**, 412 (1982).
[77]S. M. Folies, M. I. Baskes, and M. S. Daw, Phys. Rev. B **33**, 7983 (1986).